frontiers | Frontiers in Mechanical Engineering

TYPE Original Research
PUBLISHED 21 May 2025
DOI 10.3389/fmech.2025.1595832

Check for updates

OPEN ACCESS

EDITED BY
Markus Holzner,
Boku University vienne, Austria

REVIEWED BY
Isabella Schalko,
Massachusetts Institute of Technology, United States
Mirko Musa,
Swiss Federal Institute of Technology Lausanne, Switzerland

*CORRESPONDENCE
Zia Ud Din Taj,
tajz@uwindsor.ca

RECEIVED 18 March 2025
ACCEPTED 13 May 2025
PUBLISHED 21 May 2025

CITATION
Taj ZUD, Bista S and Balachandar R (2025) Passive flow control in the wake of bed-mounted cylinders: a review and new experimental insights.
Front. Mech. Eng. 11:1595832.
doi: 10.3389/fmech.2025.1595832

COPYRIGHT
© 2025 Taj, Bista and Balachandar. This is an open-access article distributed under the terms of the Creative Commons Attribution License (CC BY). The use, distribution or reproduction in other forums is permitted, provided the original author(s) and the copyright owner(s) are credited and that the original publication in this journal is cited, in accordance with accepted academic practice. No use, distribution or reproduction is permitted which does not comply with these terms.

Passive flow control in the wake of bed-mounted cylinders: a review and new experimental insights

Zia Ud Din Taj*, Sabal Bista and Ram Balachandar

Department of Mechanical, Automotive and Materials Engineering, University of Windsor, Windsor, ON, Canada

Controlling wake flow behind bed-mounted circular cylinders is required in many engineering applications. This study investigates several passive flow control mechanisms, including the use of helical strakes, meshes, foam coverings, slots, and holes. A detailed review of existing experimental and numerical studies is conducted to examine the principles, applications, and effects of each method. While extensive research exists on individual flow control techniques, comparative studies between different methods are notably lacking. Additionally, variations in approach flow conditions across studies highlight the need for a systematic evaluation under identical or near-identical inflow conditions. To address these gaps, particle image velocimetry measurements were employed to capture and compare unsteady flow dynamics in the wake of various types of bed-mounted circular cylinders. Experiments were conducted at Reynolds number of 1.45×10^4, based on the cylinder diameter. The results show that the plain cylinder's wake flow is dominated by a large recirculation region and downstream bifurcation, while the meshed cylinder shows minimal deviation from these characteristics. The cylinders with holes generate localized turbulence and spiraling flow patterns, with diminishing effects downstream. The helical strakes induce unique channelized flow and sustained turbulence downstream, whereas the single and cross-slotted cylinders enhance near-wake turbulence and velocity via high-velocity jets, particularly in the cross-slotted configuration, making it ideal for heat transfer applications. In contrast, foam-covered cylinders effectively reduce turbulence and flow fluctuations, offering potential for applications requiring flow stability and drag reduction.

KEYWORDS

wake flow control, bed-mounted cylinders, passive flow control mechanisms, particle image velocimetry, cylinder with slots, helical strakes, foam coverings

1 Introduction

1.1 Bed-mounted circular cylinders

The study of flow past bluff bodies, including circular cylinders, has long been a foundational topic in fluid mechanics, offering both theoretical insights and practical applications across a wide range of fields. It influences the design and performance of buildings, coastal structures, heat exchangers, electronics cooling, chimney stacks, bridges, and flow past automotives, where understanding wake dynamics is essential for improving

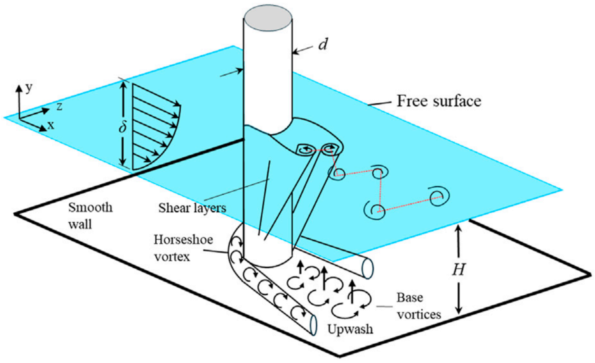

FIGURE 1
Flow features of flow past bed-mounted emergent circular cylinder [Adapted from Wang et al. (2006)]. Nomenclature: d = cylinder diameter, H = channel depth, and δ = boundary layer thickness.

efficiency and structural integrity. Numerous studies have emphasized the importance of this research, as it provides critical insights into turbulent flows and their interactions with surrounding environments (Nguyen et al., 2023; Forouzi Feshalami et al., 2022; Lekkala et al., 2022; Thompson et al., 2021; Derakhshandeh and Alam, 2019; Sumner, 2013). This field continues to be vital for developing innovative solutions to engineering challenges while advancing our understanding of such complex flow fields.

The classic case of uniform flow past circular cylinder is well understood with key flow features such as flow separation, shear layer interactions, and the formation of the well-known Kármán vortex street. These complex flow characteristics make it a valuable benchmark for developing and validating computational models. However, when a solid boundary, like a bed, is introduced—such as in the case of a wall-mounted cylinder in shallow water (Figure 1) - the flow becomes significantly more complex, exhibiting unique fluid structures and distinct patterns (Wang and Zhou, 2009). These complexities provide an opportunity to study interactions between bluff body wakes and boundary effects, which are highly relevant for real-world scenarios (Wang et al., 2006).

1.2 Shallow flows

The wake dynamics of wall-mounted bluff bodies, such as circular cylinders, are complex and influenced by factors like the approaching flow boundary layer, bed friction, free surface interactions, and flow stability. In many situations, the flow can be deemed to be shallow, which occurs when the horizontal length scale of an eddy is much larger than the vertical scale (Balachandar et al., 2000). The development of vortices in such flows is affected by the wall and the free surface. Chen and Jirka (1995) categorized shallow near-wake structures into three types—von Kármán vortex street, unsteady wake bubble, and steady wake bubble—based on the stability parameter $S = C_f d/H$, where C_f is the bed friction coefficient, d is the cylinder diameter, and H is the flow depth. Studies by Balachandar et al. (2000), Balachandar et al. (1999) showed that continuous Kármán vortices formed when $S \leq 0.008$, weak and intermittent vortices appeared for $0.009 \leq S \leq 0.018$, and vortex shedding ceased when $S > 0.021$. Akilli and Rockwell (2002) observed significant upward velocities and free surface distortions in the near wake of a cylinder in shallow water at Reynolds number $Re_H = 1 \times 10^4$. Heidari et al. (2017) further noted that both the bed and free surface significantly influence wake flow under shallow conditions, with disturbances intensifying at higher Re and Froude numbers (Fr). They proposed a modified stability parameter $S^* = (C_f + C_d)d/H$, where C_d is the drag coefficient, incorporating both bed friction and drag coefficients. Additional studies have examined the effect of free surface interactions on wake dynamics (Akilli and Rockwell, 2002; Suh et al., 2011; Kawamura et al., 2002). Suh et al. (2011) found that vortex shedding near the free surface diminishes in deep flows due to weak interaction between shear layers, while Kawamura et al. (2002) demonstrated that higher Fr amplify surface waves, intensifying their interaction with the wake.

1.3 Flow control mechanisms

Flow past a circular cylinder result in a periodic vortex shedding in the wake, leading to a drop in pressure and an increase in drag forces, as well as oscillating lift forces. These vortex-induced effects can cause structural vibrations and, in severe cases, lead to vortex-induced vibrations (VIVs) that can damage the structure (Ali et al., 2021; Ma et al., 2022; Janocha et al., 2022; Wu et al., 2022; Duranay et al., 2023; Xu and Ma, 2024; Sahu et al., 2024; Huera-Huarte, 2024). As a result, controlling vortex shedding is crucial in engineering applications to prevent such issues and improve the overall performance and durability of structures.

Among other engineering examples, flow past bed-mounted circular cylinders also resembles that around vegetation patches found in rivers and streams (Chatelain and Proust, 2021; Liu et al., 2021; Liu et al., 2022; Tariq et al., 2022; Tanaka, 2022; Kingora and Sadat, 2022; Barman and Kumar, 2022; Li et al., 2023). These interactions between fluid and vegetation create intricate flow patterns, promote turbulence, and have a significant impact on river ecosystems. Understanding how aquatic vegetation affects flow is vital for river restoration. Vegetation enhances ecology by aiding nutrient uptake, oxygen production, water purification, and filtering heavy metals like lead and mercury. The flow structure and turbulence downstream are crucial for these functions. Effective river system management thus requires a deep understanding of how the flow past cylinder modifies wake flow characteristics.

Additionally, understanding the flow characteristics and corresponding heat transfer behavior in the wake of bluff bodies is essential for developing and improving thermal management designs. Principal applications include electronic cooling systems and better thermal management systems. Flow past cylinders results in flow separation, and recirculation zones in the wake, which hinder effective heat transfer and lead to hotspots and uneven temperature distribution in cooling system designs (Terekhov, 2021; Abdollahzadeh Jamalabadi, 2021). Therefore, effective flow control mechanisms are required to address these flow and thermal challenges to disrupt stagnant flow regions, enhance turbulence, and promote better mixing in the wake.

Consequently, controlling the wake flow behind bluff bodies, especially circular cylinders, is an important aspect of engineering

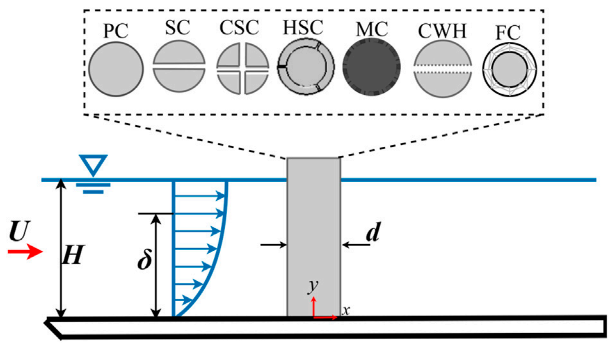

FIGURE 2
Schematic of flow past bed-mounted circular cylinders with cross-sections of the various cylinder designs with passive flow control strategies. Nomenclature: d = cylinder diameter, H = water depth, U = mean velocity, δ = boundary layer thickness, PC = plain cylinder, SC = single-slotted cylinder, CSC = cross-slotted cylinder, HSC = helical straked cylinder, MC = meshed cylinder, CWH = cylinder with holes, and FC = foam-covered cylinder.

design. This has led to the development of various techniques, which are generally classified into active and passive flow control methods. The primary goal of both active and passive techniques is to reduce drag forces, control vortex shedding, and minimize the risk of VIV, thereby enhancing the stability and service life of structures (Zhao, 2023). These techniques help prevent damage and ensure the efficient functioning of engineering systems in various applications. Active control methods, such as suction flow, cylinder oscillation, and synthetic jets, use external energy sources to manipulate fluid flow and reduce vortex shedding (Chen et al., 2022). While these methods are effective, they can be costly and energy intensive. On the other hand, passive flow control techniques focus on altering the geometry of the cylinder to achieve similar results without requiring additional energy input (Ain et al., 2022). Additionally, passive methods are often favored for their lower cost, ease of implementation, and minimal maintenance needs. Examples include the use of splitter plates, control cylinders, protrusions, helical strakes, foam coverings, slots, holes, surface dimples, roughness elements, and grooves in different orientations (Mittal and Sharma, 2021; Eydi et al., 2022; Sun et al., 2022; Zhu et al., 2023; Zeng et al., 2023; Sahu et al., 2023; Wang and Li, 2023; Muñoz-Hervás et al., 2024; Murali and Petha Sethuraman, 2024; Sikdar et al., 2024; Zhu et al., 2024; Zhao et al., 2021; Rastan and Alam, 2021; Xiao and Jing, 2024; Kusano, 2024; Roy, 2023; Priyadarsan and Afzal, 2023; Zheng et al., 2023; Yu et al., 2024; Sharma et al., 2022; Sharma and Barman, 2023; Edegbe et al., 2024).

This paper aims to examine and compare various passive flow control mechanisms for managing wake flow behind bed-mounted plain cylinder (PC) in shallow flows, including the use of helical straked cylinder (HSC), meshed cylinder (MC), foam-covered cylinder (FC), single-slotted cylinder (SC), cross-slotted cylinder (CSC), and cylinder with holes (CWH). A simple schematic of such configurations is shown in Figure 2. The detailed literature review explores the principles, applications, and effects of each technique, including both experimental and numerical studies. While extensive literature exists for individual flow control techniques, comparative studies between different methods are notably absent. Moreover, particle image velocimetry (PIV) measurements were conducted to capture unsteady flow structures in the wake of these cylinders. The PIV measurements enabled a comparison of wake characteristics with and without passive flow control techniques for optimizing wake flow in engineering applications.

The paper is arranged as follows: Section 2 discusses the current literature available on various flow control mechanisms, Section 3 shows the experimental setup used to investigate the effects on wake dynamics of circular cylinders, Section 4 provides the discussion of the results, and finally Section 5 concludes the research and provides future recommendations.

2 Review of passive flow control mechanisms

2.1 Helical straked and meshed cylinders (HSC and MC)

VIV is a significant concern in offshore engineering, particularly in the design of structures subjected to fluid flow, such as risers, pipes, and marine platforms (Duranay et al., 2023; Xu and Ma, 2024). VIV can lead to severe fatigue damage, reducing the operational lifespan of these structures and posing safety risks. As such, a wide array of techniques has been explored to mitigate VIV, with helical strakes and mesh coverings emerging as one of the most effective solutions (Korkischko and Meneghini, 2010). These devices, typically wrapped around cylindrical structures, disrupt the periodic vortex shedding that drives VIV, thereby reducing the amplitude of oscillations. In addition to VIV suppression, strakes have also been shown to affect heat transfer characteristics. The enhanced turbulence created by helical strakes can increase the convective heat transfer rate by improving the mixing of the boundary layer, leading to better thermal performance. A schematic of flow past a bed-mounted helical and meshed circular cylinders is shown in Figure 3, where h = strake height and Θ = flow incidence angle.

Numerous experimental studies have focused on the impact of helical strakes on flow past cylinders, exploring their effectiveness in reducing VIVs, listed in Table 1 (Korkischko and Meneghini, 2010; Hao et al., 2010; Zhou et al., 2010; Zhou et al., 2011; Huang, 2011; Korkischko and Meneghini, 2011; Huang and Sworn, 2013; Quen et al., 2014; Gao et al., 2014; Sui et al., 2016; Gao Y. et al., 2017; Senga and Larsen, 2017; Quen et al., 2018; Ren et al., 2019a; Ren et al., 2019b; Xu et al., 2020; Ren et al., 2020; Yadegari et al., 2023; Thakurta and Balachandar, 2025). Korkischko and Meneghini (Korkischko and Meneghini, 2010) tested different pitch and height combinations of helical strakes and found that smaller strake heights (h/d = 0.1) reduced oscillations, while h/d = 0.2 and 0.25 nearly eliminated VIV. Their observations showed that in tandem arrangements, wake interference led to galloping-like oscillations. Using stereoscopic digital particle image velocimetry (SDPIV), their study highlighted how strakes disrupted vortex shedding and controlled out-of-plane flow. Building on this, Hao et al. (2010) further explored vortex structures using hot film and PIV measurements in the wake of HSC. Using a triple strake system with varying h/d, they found significant VIV suppression, especially

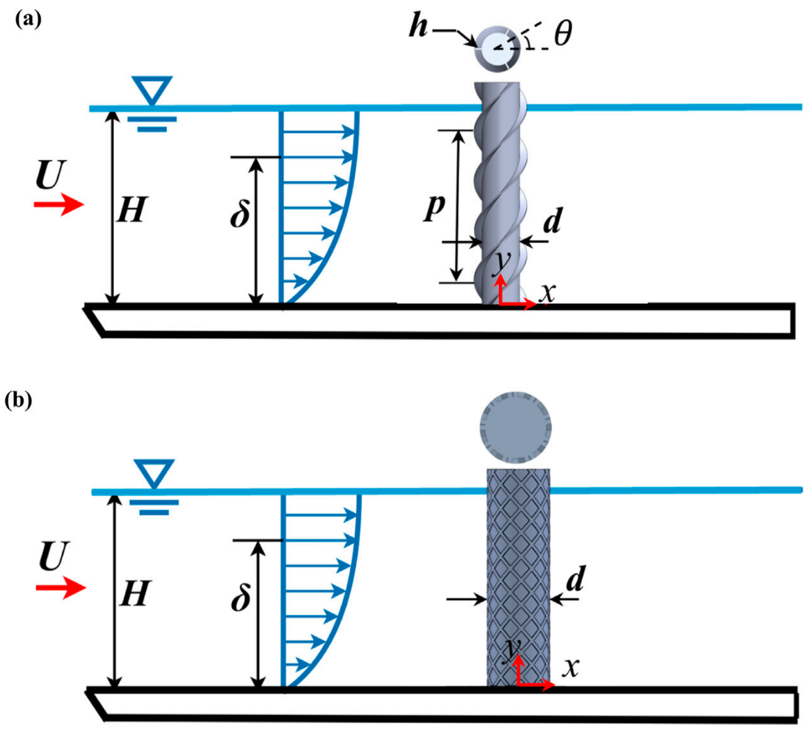

FIGURE 3
Schematic of flow past a bed-mounted **(a)** helical straked circular cylinder and **(b)** meshed circular cylinder. Nomenclature: h = strake height, p = strake pitch, and Θ = flow incidence angle.

with h/d = 0.2, leading to a more stable wake and weakened vortex shedding.

Similarly, Zhou et al. (2010), Zhou et al. (2011) conducted wind tunnel experiments on HSC, demonstrating up to 98% VIV reduction. The strakes eliminated lock-in behavior and weakened vortex shedding, causing phase mismatches along the cylinder's height. This was further supported by velocity measurements, which showed significant variations in the dominant vortex frequency. Huang (2011) also focused on VIV suppression and drag reduction, showing a 64% reduction in VIV amplitude and a 25% drag reduction for fixed cylinders, underscoring the dual benefits of helical structures. Similarly, Korkischko and Meneghini (2011) used a two-camera stereoscopic PIV system to investigate the flow behind HSC. They found that strake pitch (p/d) of 10 and height (h/d) of 0.1 and 0.2 introduced a defined wavelength in the wake, which increased vortex formation length—critical for VIV suppression. In addition, Huang and Sworn (2013) explored the hydrodynamic coefficients of stationary HSC in staggered and tandem positions. While strakes increased drag, they significantly reduced fluctuating forces on the upstream cylinder, although the effect was less pronounced on the downstream cylinder.

Quen et al. (2014) extended this research to flexible risers, showing that strakes with heights greater than the laminar boundary layer thickness were most effective in reducing VIV. They also found that p/d influenced the occurrence of lock-in, while increasing h/d narrowed the lock-in region. Strakes proved more effective for rigid cylinders than flexible ones, though drag penalties were observed at higher reduced velocities. Gao et al. (2014) further confirmed that VIV suppression depended heavily on h/d and noted that strakes significantly reduced fatigue damage in the crossflow direction, although drag increased with both pitch and height. Expanding on these findings, Sui et al. (2016) focused on a flexible cylinder with large mass-damping parameters at Re = 2.7×10^3 and 57.9×10^3, finding that strake height and coverage were the most significant factors for VIV suppression, with the optimal configuration of p/d = 5 and h/d = 0.14 achieving over 85% suppression efficiency, and up to 98% at a reduced velocity U_r = 20, where $U_r = U_o/f_n d$, U_o and f_n are the free stream velocity and natural frequency of the cylinder, respectively. Flow visualizations confirmed that strakes altered shear layer interactions, reducing vortex scale and vortex shedding. In a similar manner, Gao Y. et al. (2017) studied flexible risers with helical strakes under uniform and linearly sheared currents. They found that strake coverage played a crucial role in VIV suppression, with configurations of 75% and 50% coverage being optimal for uniform and sheared currents, respectively, effectively reducing fatigue damage.

On the other hand, Senga and Larsen (2017) investigated the hydrodynamic coefficients of HSC through forced motion experiments—where controlled oscillations were applied to the test cylinder using a computer-controlled towing carriage equipped with a motion simulator and load cells for force measurement—and observed significant differences in drag and added mass coefficients compared to bare cylinders. These findings demonstrated how helical strakes disrupt vortex shedding and enhance flow stability. Similarly, Quen et al. (2018) examined two- and three-start helical strakes on a flexible cylinder, revealing that three-start strakes were more effective in reducing VIV amplitude. The best configuration involved a three-start strake

10.3389/fmech.2025.1595832

TABLE 1 Previous experimental and numerical studies on flow past helical straked and meshed circular cylinders. Nomenclature: p = strake pitch and h = strake height.

Author(s) (year)	Re_d (x 10^{-3})	Number of helix, n	Pitch, p/d	Height, h/d
(A) Experiments				
Korkischko and Meneghini (2010)	1–10	3	5, 10, 15	0.1, 0.2, 0.25
Hao et al. (2010)	2.4, 4.8, 7.2	3	25	0.1, 0.2
Zhou et al. (2010)	10.2–40.8	3	10	0.12
Zhou et al. (2011)	10.2–40.8	3	10	0.12
Huang (2011)	13–46	3	6	0.15, 0.2
Korkischko and Meneghini (2011)	1, 10	3	10	0.1, 0.2
Huang and Sworn (2013)	14–42.1	3	10	0.1
Quen et al. (2014)	1.38–13.8	3	5, 10, 15	0.05, 0.1, 0.15
Gao et al. (2014)	9.2–73.8	3	5, 17.5, 20	0.1, 0.15, 0.25
Sui et al. (2016)	2.7–57.9	3	5–17.5	0.1–0.3
Gao et al. (2017a)	3.1–36.6	3	16	0.25
Senga and Larsen (2017)	14–17	3	5, 17.5	0.14, 0.25
Quen et al. (2018)	1.38–13.8	2, 3	5, 10, 15	0.05, 0.1, 0.15
Ren et al. (2019a)	5.24–15.7	3	15	0.25
Ren et al. (2019b)	11–95	3	5, 17.5	0.1–0.3
Xu et al. (2020)	0.8–16	3	17.5	0.25
Ren et al. (2020)	5.2–10.5	3	15	0.25
Yadegari et al. (2023)	10, 40	3	3	0.05, 0.07
Thakurta and Balachandar (2025)	7	3	10	0.2
(B) Computational fluid dynamics simulations				
Constantinides and Oakley (2006)	200–1,000	3	15	0.25
Carmo et al. (2012)	1	3	10	0.2
Ranjith et al. (2016)	0.1, 28	3	10	0.15
Chen et al. (2019)	0.2–16	1, 2, 3	5, 10, 15	0.05, 0.1, 0.2
Ishihara and Li (2020)	16–24.5	4	8	0.1

with $p/d = 10$ and $h/d = 0.15$, emphasizing the importance of strake configuration in VIV suppression. Ren et al. (2019a), Ren et al. (2019b) studied VIV suppression in flexible pipes fitted with helical strakes in oscillatory flow and found that while strakes were effective in steady flow, their efficiency decreased in unsteady conditions. They also highlighted the impact of strakes on drag coefficients in uniform flow, noting that $p/d = 5$ reduced mean drag coefficients while simultaneously suppressing VIV. Xu et al. (2020) expanded on this by exploring the performance of helical strakes on two side-by-side flexible cylinders. They found that strakes effectively reduced VIV in both single and multi-cylinder configurations, suggesting their applicability in complex offshore systems. In contrast, Ren et al. (2020) examined hydrodynamic coefficients in oscillatory flow and showed that strakes increased drag, underlining the need to balance VIV suppression with potential drag penalties in unsteady flows. Yadegari et al. (2023) studied the wake characteristics of HSC at $Re = 1 \times 10^4$ and 4×10^4, observing a reduction in turbulence intensity and shifts in the critical Re for vortex shedding, which contributed to improved stability by altering the wake structure. Similarly, Thakurta and Balachandar (2025) investigated wake dynamics of wall-mounted HSC in shallow flow, finding that strakes increased turbulence levels and influenced vortex formation, with strake orientation (θ) affecting Reynolds stresses and wake mixing, potentially optimizing VIV reduction in wall-mounted structures.

In addition to these experimental findings, several computational studies have also explored the effects of helical strakes on VIV suppression, listed in Table 1 (Constantinides and Oakley, 2006; Carmo et al., 2012; Ranjith et al., 2016; Chen et al., 2019; Ishihara and Li, 2020). Constantinides and Oakley (Constantinides and Oakley, 2006) used a second-order finite element computational fluid dynamics (CFD) method to simulate

10.3389/fmech.2025.1595832

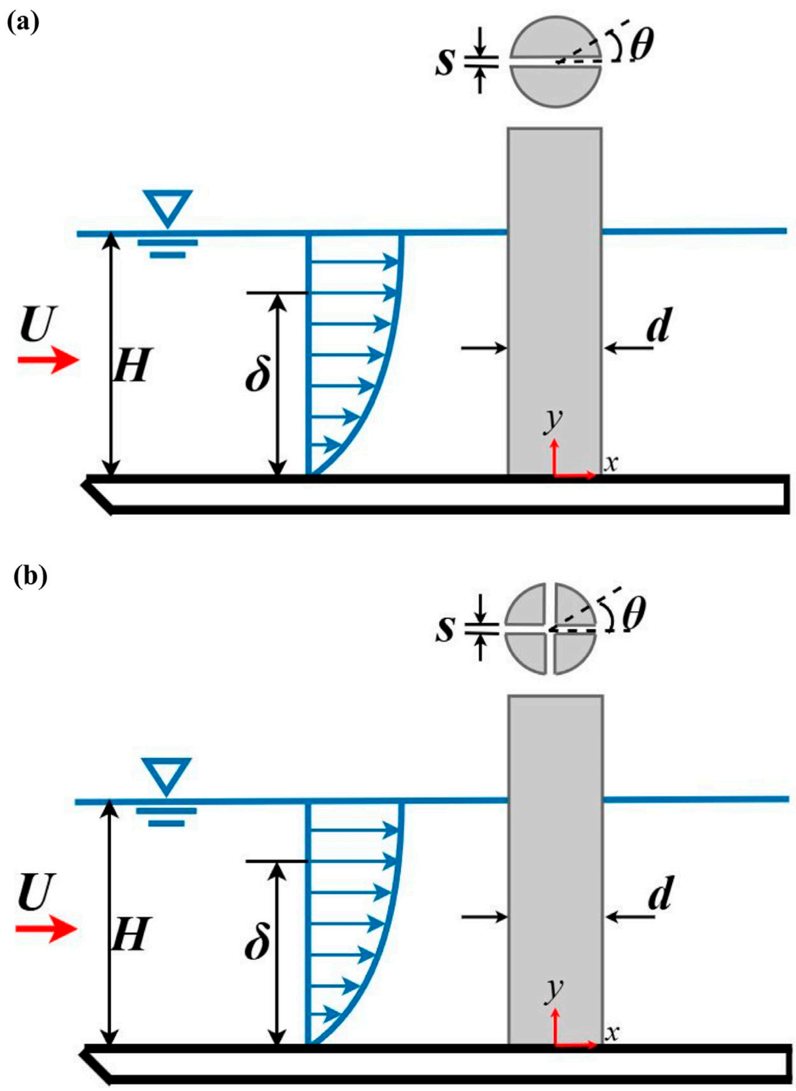

FIGURE 4
Schematic of flow past a wall-mounted **(a)** single-slotted cylinder and **(b)** cross-slotted cylinder. Nomenclature s = slot width and Θ = flow incidence angle.

VIV of bare and straked cylinders. They compared two turbulence models—Spalart-Allmaras Reynolds Averaged Navier Stokes (RANS) modelling and detached eddy simulation (DES)—and found that strakes effectively mitigated VIV by disrupting vortex shedding, with DES providing more accurate results than RANS. Carmo et al. (2012) utilized two- and three-dimensional (2D and 3D) simulations using spectral element method to study flow around cylinders with strakes. Their results showed that while 2D simulations were ineffective at suppressing vibrations, 3D simulations demonstrated that strakes reduced vortex shedding correlation along the span and altered vortex wake formation, thereby improving VIV suppression. Similarly, Ranjith et al. (2016) numerically examined the effects of three-strand helical strakes on VIV suppression for a rigid circular cylinder at $Re = 0.1 \times 10^3$ and 28×10^3 with $p/d = 10$ and $h/d = 0.15$. Their results showed that while helical strakes increased drag, they reduced VIV by nearly 99%, highlighting their effectiveness in stabilizing the flow and suppressing vortex shedding.

Expanding on this work, Chen et al. (2019) conducted 3D CFD simulations to investigate helical strakes' impact on VIV suppression in flexible risers. They found that strakes disrupted vortex structures and reduced vortex shedding frequency, achieving a 97% reduction in transverse vibration at a reduced velocity of 7. In a similar manner, Ishihara and Li (2020) studied VIV suppression in HSC using a large eddy simulation (LES) model. Their study showed that helical wires reduced VIV amplitude by nearly 80%, primarily by enhancing 3D disturbances in the wake, thus reducing fluctuating lift forces and improving aerodynamic damping. While the effectiveness of helical strakes in mitigating VIV has been consistently demonstrated across a wide range of experimental and numerical studies, the effect on heat transfer rates due to the vortical structures responsible for enhanced turbulence still needs to be explored.

TABLE 2 Previous experimental and numerical studies on flow past single-slotted circular cylinders.

Author(s) (year)	Re_d (10^3)	Flow incidence angle, Θ (degrees)	Slot size, s/d
(A) Experiments			
Igarashi (1978), Igarashi (1982)	13.8–52	0°–90°	0.08, 0.185
Olsen and Rajagopalan (2000)	0.06–2.3	0°–90°	
Fu and Rockwell (2005)	18	0°	0.016–0.125
Peng et al. (2012)	2.4–85	90°	0.05–0.3
Ordia et al. (2017)	0.2–2.3	0°	0.1, 0.2, 0.4
Gao et al. (2017b)	26.7	0°	0.05–0.15
Gao et al. (2017c)	26.7	0°–90°	0.075
Kim et al. (2023)	32	0°–90°	0.1
Boamah (2024)	14.5	0°–90°	0.1
(B) Computational fluid dynamics simulations			
Baek and Karniadakis (2009)	0.5, 1	0°	0 to 0.3
Jian Sheng and Chen (2016)	0.06–0.25	0°	0.1–0.3
Wang and Wang (2016)	3.7	0°	0.35
Ma and Kuo (2016)	0.2	90°	0.03–0.3
Bao et al. (2018)	0.2	0°–90°	0–0.3

2.2 Single-slotted cylinders (SC)

Another method to modify and control the flow separation and wake dynamics is the use of slots. The flow from the slot acts as a jet in the wake region, disrupting stagnant flow regions and increasing turbulence. This helps in controlling wake to reduce vortex formations and improving heat transfer in various engineering designs. A schematic of flow past a bed-mounted slotted circular cylinder is shown in Figure 4a, where s = slot width and Θ = flow incidence angle. Researchers have conducted numerous experimental studies in the past for examining the flow past single slots due to its effectiveness as a passive flow control mechanism (see Table 2). (Igarashi, 1978; Igarashi, 1982; Olsen and Rajagopalan, 2000; Fu and Rockwell, 2005; Peng et al., 2012; Ordia et al., 2017; Gao et al., 2017b; Gao et al., 2017c; Kim et al., 2023; Boamah, 2024) An early experimental study was conducted by Igarashi (1978), Igarashi (1982), who examined the flow characteristics around SC. The findings revealed that θ significantly influenced flow behavior. For $0° \leq \theta \leq 40°$, self-injection into the wake was observed, raising the base pressure and moving the vortex formation region downstream. For θ values beyond 60°, periodic boundary layer suction was observed, reducing the base pressure coefficient and vortex shedding frequency. These studies laid a foundation for understanding flow control using slots.

Building on this foundation, further investigations by Olsen and Rajagopalan (2000) explored vortex shedding in SC and concave rear notches. They noted distinct differences in the Strouhal number and drag coefficient compared to plain cylinders. For a cylinder with a slot normal to the flow, the drag coefficient reached 1.41, higher than the baseline case. Stable vortex shedding patterns were observed at specific Reynolds numbers, providing insights into modifying wake structures. In another study, Fu and Rockwell (2005) examined shallow flow past a cylinder with base bleed through a narrow slot using PIV measurements, demonstrating its ability to delay vortex formation significantly. The delayed vortex formation was attributed to the interaction between the base bleed and near-wake flow structures.

Peng et al. (2012) expanded this understanding by focusing on vortex shedding from SC in both wind tunnel and water channel experiments. They found an optimal range of s/d = 0.1–0.15, where vortex shedding signals exhibited high quality and two-dimensionality. The linear Strouhal-Reynolds number relationship within this range underscored the role of slot in maintaining flow coherence across Re. Complementing these findings, Ordia et al. (2017) visualized flow past SC and revealed unique wake behaviors, including symmetric and anti-phase vortex shedding. At higher s/d, the configuration acted as two different bodies, producing increased vortex shedding.

Gao et al. (2017b), Gao et al. (2017c) extended the exploration by studying flow characteristics around SC at various θ, using PIV to quantify wake modifications. A slot at low θ effectively reduced drag and suppressed lift fluctuations. At higher angles, boundary layer suction and blowing became dominant, delaying flow separation and shrinking the wake width. Recently, Kim et al. (2023) investigated the combined effects of slots and axially arranged holes on flow control. The passive jet from the leeward side pushed the wake vortex downstream, reducing drag at smaller θ. However, at larger angles, alternate blowing and suction promoted boundary layer transition, shortening shear layers and increasing drag. In a related study, Boamah (2024) examined the effect of θ on SC wake flow in shallow conditions. PIV measurements showed varying wake characteristics, with jet momentum decreasing as θ

increased from 0° to 30°. At higher angles, shear layer interactions intensified, shifting peak Reynolds shear stress closer to the bluff body.

Similarly, researchers have conducted numerous numerical studies to highlight the effectiveness of slots as passive flow control mechanisms, listed in Table 2 (Baek and Karniadakis, 2009; Jian Sheng and Chen, 2016; Wang and Wang, 2016; Ma and Kuo, 2016; Bao et al., 2018). By altering wake structures, delaying separation, and modifying vortex dynamics, slots enable enhanced aerodynamic performance and flow management across a wide range of applications. For instance, Baek and Karniadakis (2009) conducted simulations using spectral element method to investigate the hydrodynamic effect of SC to minimize VIV without energy consumption. The slot, positioned parallel to the incoming flow, effectively suppressed VIV by weakening or detuning vortex shedding. At $Re = 5 \times 10^2$, the optimal slot size was identified, with smaller sizes required at $Re = 1 \times 10^3$. Larger s/d, however, caused increased jet-like flow, altering the vortex shedding behaviour. Stability analysis revealed changes in wake stability, inducing regions of absolute and convective instability.

Building on this, Jian Sheng and Chen (2016) explored the impact of a slot positioned along the diameter of a circular cylinder for drag reduction and vortex suppression. The study demonstrated that drag reduction occurred by diverting fluid from the front stagnation region to the low-pressure zone behind the cylinder. In the range of $Re = 0.6 \times 10^2$–2.5×10^2, increasing the slot width ratio reduced both drag and lift coefficients, while vortex shedding from the slot altered the wake flow, shifting vortex formation further downstream. Further investigations into heat transfer and flow were conducted by Wang and Wang (2016), who examined a rectangular channel with SC using LES at $Re = 3.7 \times 10^3$. The interaction between the cylinder's wake and the boundary layer significantly improved heat transfer. Compared to a plain cylinder, the impinging jet from the slot enhanced wake and boundary layer interaction.

Additionally, Ma and Kuo (2016) conducted 2D flow simulations around a circular cylinder with a normal slot at $Re = 2 \times 10^2$. They examined slot ratios ranging from $s/d = 0.03$ to 0.3 and found that periodic blowing and suction at the slot delayed boundary-layer separation and shortened the vortex formation length. *At* $s/d = 0.18$, optimal synchronization between slot flow and vortex-street formation resulted in primary lock-on of the wake. Lastly, Bao et al. (2018) studied SC at low Re, varying s/d from 0 to 0.3 and θ from 0° to 90°. For angles between 0° and 45°, larger s/d and smaller angles resulted in reduced drag and lift coefficients, with a maximum drag reduction of 28.6% at $s/d =$ 0.30 and $\theta = 0°$. However, for angles between 60° and 90°, drag and lift coefficients increased due to strengthened and stabilized vortex patterns. Despite these comprehensive studies on flow field characteristics, there remains a lack of detailed experimental and numerical investigations examining the corresponding effects of slotted cylinders in heat transfer applications.

2.3 Cross-slotted cylinders (CSC)

Building on the work done on single slots, researchers have explored the use of multiple slotted cylinders in modifying the flow characteristics, suppress vortex shedding, reducing drag, and enhancing heat transfer. A schematic of flow past a bed-mounted slotted circular cylinder is shown in Figure 4b, where s = slot width and Θ = flow incidence angle. As compared to the single slots, the literature on the flow past multiple slotted cylinders is limited, listed in Table 3 (Shi and Feng, 2015; Chen et al., 2023; Taj et al., 2024; Wang and Dong, 2017; Zhu et al., 2019). Researchers have conducted few experimental studies to examine the effectiveness of multiple slots as a passive flow control mechanism to modify wake dynamics, improve aerodynamic performance, and enhance heat transfer (Shi and Feng, 2015; Chen et al., 2023; Taj et al., 2024). For example, Shi and Feng (2015) explored flow control around a circular cylinder using bleed jets near the separation points. Their study revealed that s/d had a substantial impact on wake dynamics, with larger slots increasing vortex formation length and reducing vortex shedding frequency, leading to a more stable vortex pattern.

Building on this, Chen et al. (2023) examined the wake dynamics of a circular cylinder with two perpendicular slots at $Re = 1.8 \times 10^3$. Their results showed that the introduction of slots altered vortex shedding behavior, reduced drag, and shifted vortex formation downstream. Further advancing the understanding of CSC configurations, Taj et al. (2024) investigated the wake dynamics of a wall-mounted CSC in a shallow water channel at $Re = 1.45 \times 10^4$. Their findings showed that the cross-slot configuration accelerated the flow behind the cylinder, moving the recirculation region downstream and increasing turbulence in the near wake. This increased turbulence impacts heat transfer, suggesting that cross-slotted cylinders could offer a promising solution for thermal management by reducing temperatures in heat-accumulated areas near the wake.

In a numerical context, Wang and Dong (2017) studied the flow and heat transfer characteristics of a multiple slotted cylinder. Their results showed that increasing s/d suppressed vortex shedding, reduced drag and lift coefficients, and improved heat transfer performance. Notably, the transition from 2D to 3D vortex shedding was influenced by s/d, further emphasizing the role of slot geometry in improving flow behavior and thermal performance. Moreover, Zhu et al. (2019) conducted direct numerical simulations of flow over a multiple slotted cylinder at a low $Re = 1 \times 10^2$. They compared several slot types, including streamwise, T-shaped, Y-shaped, and transverse slots. Their findings showed that the transverse slot was the most effective in reducing drag and lift forces, stabilizing vortex shedding, and improving overall flow dynamics.

Furthermore, Alshareef et al. (2022) examined cylinders with orthogonal and parallel slots under transverse flow for $Re = 1 \times 10^2$ and 10×10^2. They found that slotted cylinders achieved significant heat transfer improvements—up to 81% for orthogonal slots and 100% for parallel slots—due to the increased surface area. Despite additional viscous drag, total drag force was reduced by up to 30%. The performance index, representing the ratio of heat transfer to drag force, showed the best results for parallel slots, with values reaching up to 2.8. Recently, Alhashem et al. (2024) focused on V-shape slotted cylinders, where drag reduction reached up to 67% at $s/d = 0.2$. Heat transfer improved with increasing s/d, peaking at an enhancement of 192% at $s/d = 0.15$ before declining. The optimal performance index occurred at $s/d = 0.175$. However, detailed numerical and experimental investigations of the effect of various

TABLE 3 Previous experimental and numerical studies on flow past multiple slotted circular cylinders.

Author(s) (year)	Re_d (10^3)	Flow incidence angle, ϴ (degrees)	Slot size, *s*/*d*
(A) Experiments			
Shi and Feng (2015)	0.4, 0.78, 1.5	45°	0.05, 0.1, 0.2
Chen et al. (2023)	1.8	0°, 22.5°, 45°	0.08
Taj et al. (2024)	14.5	0°	0.1
(B) Computational fluid dynamics simulations			
Wang and Dong (2017)	0.22–0.26	82°	0.02–0.1
Zhu et al. (2019)	0.1	0°, 60°, 90°	0.075
Alshareef et al. (2022)	1.1–1	0°	0.1–0.2
Alhashem et al. (2024)	0.5	0°	1.1–0.2

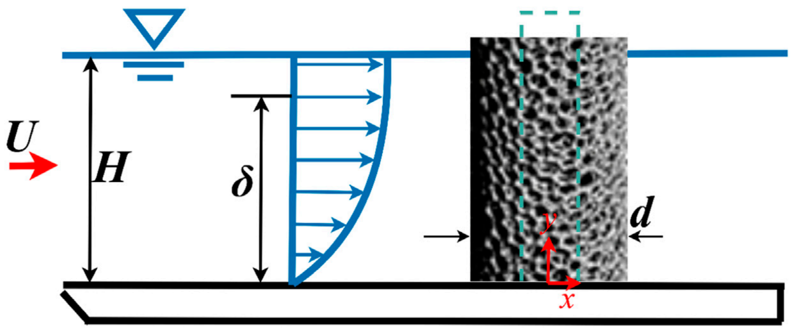

FIGURE 5
Schematic of flow past a bed-mounted foam-covered circular cylinder.

parameters like θ, Re, and s/d for the case of CSC is needed as observed in the case of SC.

2.4 Foam-covered cylinders (FC)

The addition of a foam covering alters flow and turbulence patterns by interrupting large-scale structures and minimizing flow-induced oscillations, which can otherwise compromise structural integrity (Bruneau and Mortazavi, 2008). Porous media provide a passive method for wake flow control while protecting the main body by introducing an alternate flow zone that separates the structure from oscillations. This intermediate zone breaks up large-scale vortices, reduces vortex shedding frequency, and minimizes VIV. Additionally, FC reduce aerodynamic drag, offer shelter for aquatic habitats, and find applications in filters, mixers, heat exchangers, and environmental studies like aquatic vegetation flows and fish passages near hydraulic structures (Arbak and Dukhan, 2020; Li et al., 2021; Boules et al., 2021; Freitas et al., 2022; Hu et al., 2023).

A schematic of flow past a bed-mounted foam-covered circular cylinder is shown in Figure 5. FC comprises an inner solid cylinder wrapped in highly porous foam. Fluid flows through the porous region, emerging from the sides or rear end while vertical bleeding is restricted by the enclosing plates. This porous flow creates an intermediate velocity zone, shielding the wake of the inner cylinder and delaying shear layer roll-ups, which extend the recirculation region. The foam structure further stretches this region, carrying fluid downstream and reattaching to the bottom wall over a longer distance.

The addition of porous or foam materials to the surface of cylinders has been investigated experimentally in the past to modify flow characteristics (Sueki et al., 2010; Zong and Nepf, 2012; Ashtiani Abdi et al., 2014; Yuan et al., 2016; Klausmann and Ruck, 2017; Ashtiani Abdi et al., 2017; Xia et al., 2018; Du et al., 2022; Xu et al., 2023; Das et al., 2023). For example, Sueki et al. (2010) explored the application of porous materials using PIV to reduce aerodynamic sound from bluff bodies. Their experiments revealed a significant reduction in aerodynamic sound for porous-coated cylinders due to suppressed vortex shedding and stabilized shear layers. Surface pressure distribution and aerodynamic force fluctuations were altered, reducing unstable vortex motion, widened zero-velocity regions and reduced vortex shedding intensity. Similarly, Zong and Nepf (2012) studied the wake behind porous circular obstructions in a channel, mimicking vegetation. They found a steady wake region downstream, with length increasing with porosity ($1 - \varnothing$, where $\varnothing$ is the solid volume fraction), delaying the von Kármán vortex street formation. Elevated transverse velocity fluctuations occurred near the obstruction and at downstream locations where large-scale oscillations began. Porosity significantly altered wake structures and delayed vortex formation.

Ashtiani Abdi et al. (2014) used hot-wire anemometery (HWA) technique to investigate heated FC across $Re = 1 \times 10^3 - 10 \times 10^3$. Heating influenced flow instability and vortex shedding, with increased surface turbulence reducing pressure drop and enhancing heat transfer. Porous materials modified both flow behavior and thermal properties. Further extending the experimental understandings, Yuan et al. (2016) studied finite circular cylinders with porous coatings using HWA, revealing reduced vortex shedding frequency and expanded wake regions. Porous coating stabilized the boundary layer, suppressed Kelvin-Helmholtz instability, and delayed shear layer roll-up, leading to weaker shear layer interactions and more stable flow. In another experimental study using laser Doppler anemometry (LDA), Klausmann and Ruck (2017) examined drag reduction via porous coatings on the leeward side of circular cylinders. Experiments showed a maximum drag reduction of 13.2% at subcritical *Re*. Porous coatings reduced pressure fluctuations and shifted vortex formation downstream, reconfiguring the wake region and diminishing aerodynamic forces. Additionally, Ashtiani Abdi et al. (2017) compared flow structures downstream of foamed and bare tubes using PIV. Experiments at $Re = 4 \times 10^3$ and 16×10^3 showed increased three-dimensionality of flow in the streamwise direction for foamed tubes, with elongated flow structures downstream. Spanwise and normal directions exhibited minimal structural changes.

Xia et al. (2018) used HWA, PIV, and smoke-wire visualization to study wake dynamics of porous-coated cylinders. Results indicated reduced Reynolds stresses, elongated vortex formation length, and widened wake regions. Proper orthogonal decomposition (POD) analysis revealed weakened asymmetrical vortex shedding for porous coatings, with symmetric modes gaining prominence. Moreover, Du et al. (2022) investigated drag reduction using porous materials of varying permeability on cylinder surfaces. Experiments showed a maximum drag reduction of 10.21% with optimized porous material placement. Flow visualization indicated expanded vortex regions, reduced shedding frequency, and dissipated vorticity. Furthermore, Xu et al. (2023) examined pressure drag and aerodynamic noise for cylinders with porous coatings. Experimental results showed that porous coatings suppress near-field pressure fluctuations and far-field noise. Key parameters, including pore density and coating thickness, were analyzed to optimize drag and noise reduction. Recently, Das et al. (2023) studied wake characteristics of FC using LES validated by PIV. Foam coverings interrupted large periodic structures, suppressed lateral oscillations, and shifted vortex regions downstream. Spectral analysis highlighted reduced dominant frequencies and modified recirculation regions.

Similarly, researchers have conducted numerous numerical studies to highlight the effect of foam coverings on fluid dynamics and heat transfer, listed in Table 4 (Das et al., 2023; Bhattacharyya et al., 2006; Bhattacharyya and Singh, 2011; Odabaee et al., 2011; Liu et al., 2014; Chang et al., 2017; Arcondoulis et al., 2019). For instance, Bhattacharyya et al. (2006) investigated flow past FC using numerical simulations. They examined $Re = 1$ and 40, with Darcy numbers in the range of 10^{-6} to 1.5. Their results showed that increasing Darcy numbers reduced drag coefficients, altered separation angles, and influenced recirculation lengths. Similarly, Bhattacharyya and Singh (2011) performed a numerical investigation using a porous covering. They explored the effects of porous layer thickness and permeability, revealing significant drag reduction and oscillation damping. The study demonstrated that optimal porous layer characteristics can suppress vortex shedding and stabilize the wake.

Furthermore, Odabaee et al. (2011) conducted numerical simulations on heat transfer augmentation from a metal FC in crossflow. They found an optimal porous layer thickness for maximizing heat transfer while minimizing pressure drop. Results showed higher heat transfer rates compared to finned-tube heat exchangers, emphasizing the effectiveness of metal foam coatings. Likewise, Liu et al. (2014) analyzed flow past FC using unsteady RANS simulations. They demonstrated that porous coatings mitigated aerodynamic force fluctuations, suppressed vortex shedding, and reduced mean drag. The sensitivity of aerodynamic forces to coating thickness was highlighted, showing its importance in flow-induced noise reduction and aerodynamic optimization. Building on this, Chang et al. (2017) examined the effects of solid volume fraction, relative cylinder diameter, turbulence structures, and sediment erosion using DES. Their findings provided insights into wake dynamics and sediment transport in vegetative flows. Lastly, Arcondoulis et al. (2019) designed structured porous materials for passive flow and noise control around cylinders. The results demonstrated the effectiveness of 3D-printed porous coatings in reducing vortex shedding tones and aerodynamic noise. The structured porous design showed potential for further optimization and tailored flow control applications. While foam-covered cylinders have shown promise in attenuating vortex shedding and suppressing wake instabilities, comprehensive studies investigating the unsteady wake dynamics—particularly at higher *Re*—remain limited.

2.5 Cylinders with holes (CWH)

Although introducing slots along the entire span of the cylinder has proven effective in altering flow behavior, increasing the slot width to enhance performance often compromises the structural integrity of the model. Similarly, a continuous slot along the cylinder weakens the body's overall stability. To address these limitations, an array of holes drilled through the cylinder offer an alternative. This approach retains the advantages of passive flow control while maintaining the structural strength of the model, making it a practical solution for engineering applications. A schematic of flow past a bed-mounted CWH is shown in Figure 6, where d_h = hole diameter, s_h = distance between consecutive holes, and $\boldsymbol{\Theta}$ = flow incidence angle. A limited literature is available for the flow past CWH, listed in Table 5 (Kim et al., 2023; Yajima and Sano, 1996; Firat et al., 2017; Clapperton and Bearman, 2018; Firat et al., 2019). For instance, Yajima and Sano (Yajima and Sano, 1996) showed that two arrays of holes across the diameter of a hollow circular cylinder led to significant drag reduction of up to 40% at $Re = 5 \times 10^3$ and 9×10^3. Their study demonstrated the potential of hole configurations in reducing drag across a range of attack angles. Firat et al. (2017) investigated the wake behind cylinders with two rows of holes at a $Re = 6.9 \times 10^3$, varying hole diameter ratio (d_h/d) and hole-to-hole gap ratio (s_h/d). They found that larger hole

TABLE 4 Previous experimental and numerical studies on flow past foam-covered circular cylinders.

Author(s) (year)	Re_d (10^3)	Pores per inch (*ppi*)	Porosity (1 – ∅)
(A) Experiments			
Sueki et al. (2010)	46, 83	13	0.97
Zong and Nepf (2012)	22–41	—	0.64–0.97
Ashtiani Abdi et al. (2014)	1–10	10	0.95
Yuan et al. (2016)	8	10–30	—
Klausmann and Ruck (2017)	35–140	20	—
Ashtiani Abdi et al. (2017)	4, 16	10	—
Xia et al. (2018)	100	13	0.97
Du et al. (2022)	13.5–67.5	20–80	0.95
Xu et al. (2023)	100–200	40–80	0.85
Das et al. (2023)	13	—	0.95
(B) Computational fluid dynamics simulations			
Bhattacharyya et al. (2006)	0.001–0.04	—	0.629–0.999
Bhattacharyya and Singh (2011)	0.04–0.2	—	0.9
Odabaee et al. (2011)	9.7–19.4	—	0.9–0.95
Liu et al. (2014)	47, 90	—	0.97
Chang et al. (2017)	0.48–0.96	—	0.77–0.908
Arcondoulis et al. (2019)	80–150	10	0.87, 0.9, 0.95
Das et al. (2023)	13	—	0.95

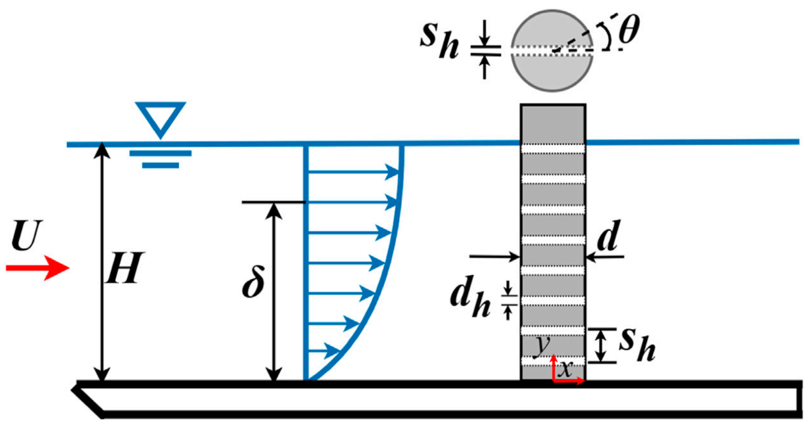

FIGURE 6
Schematic of flow past a bed-mounted circular cylinder with holes. Nomenclature: d_h = hole diameter, s_h = distance between consecutive holes, and Θ = flow incidence angle.

diameters increased jet momentum, leading to an expanded recirculation region and shifted vortex formation. These changes affected the shear layers and vortex shedding patterns, showing that hole configuration significantly modifies wake behavior and contributes to drag reduction.

Clapperton and Bearman (2018) examined passive jets generated through spanwise holes at $Re = 3 \times 10^4$ to 28×10^4. They found that these jets delayed flow separation and suppressed vortex shedding, resulting in a 14.5% drop in drag from the baseline cylinder. Their study highlighted the role of passive jets in flow control and drag reduction. In a subsequent study, Firat et al. (2019) explored cylinders with holes at ± 90° from the front stagnation line. Their findings showed that this configuration acted like a synthetic jet actuator, producing a

TABLE 5 Previous experimental studies on circular cylinders with holes.

Author(s) (year)	Re_d (10^3)	Diameter ratio, d_h/d	Hole-to-hole gap, s_h/d
(A) Experiments			
Yajima and Sano (1996)	5–9	0.09	0.1875
Firat et al. (2017)	6.9	0.1, 0.15, 0.20	0.2–1.4
Clapperton and Bearman (2018)	30–280	0.005, 0.01	0.1, 0.2
Firat et al. (2019)	6.9, 20	0.2	1.4
Kim et al. (2023)	32	0.1	0.13, 0.18, 0.23

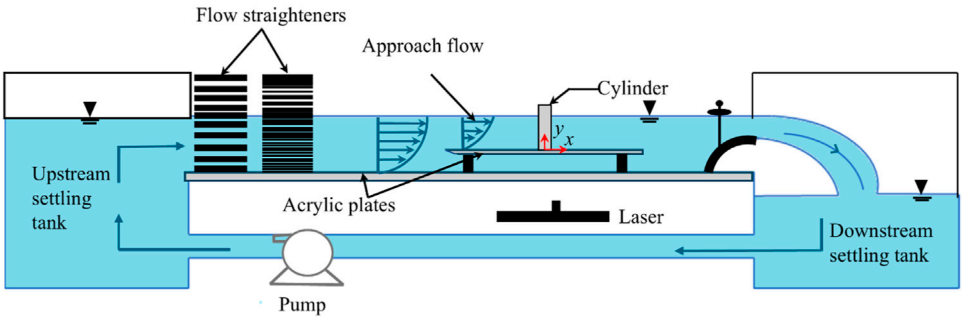

FIGURE 7
Experimental setup [Adapted from Das et al. (2023)].

14.4% drag reduction. They also identified how the holes initiated 3D instabilities in the wake, further influencing drag and flow characteristics. Kim et al. (2023) studied flow control over cylinders using a slot and holes at $Re = 3.2 \times 10^4$. They observed that at small incidence angles, θ, the passive jet reduced drag by pushing the wake vortex downstream. However, when θ increased beyond a critical threshold, alternate blowing and suction led to boundary-layer transitions, increasing drag. The study emphasized the importance of θ in optimizing flow control. While a few experimental studies, as discussed above, are available, detailed numerical investigations of the flow field around CWH are lacking in the literature.

The detailed literature review explored the principles, applications, and effects of various passive flow control mechanisms for managing wake flow behind bed-mounted PCs, incorporating both experimental and numerical studies. While extensive research exists on individual flow control techniques, comparative studies between different methods are notably lacking. Additionally, the literature reveals variations in approach flow conditions across studies. Therefore, there is a need to evaluate and compare the wake flow characteristics of these passive mechanisms under identical or near-identical inflow conditions.

3 New experiments

PIV experiments were conducted in a recirculating water flume at the University of Windsor (shown in Figure 7). (Thakurta and Balachandar, 2025; Das et al., 2023) The flume has a rectangular cross-section with 16 m length, 1.2 m width, and 0.8 m height. The side and bottom walls of the flume are made from transparent Plexiglas, allowing optical access to the flow. To minimize inflow disturbances, upstream settling chambers consisting of three honeycomb flow straighteners are placed at the entrance of the channel. The flow straighteners, 1 m apart, are located well ahead of the measurement section. To regulate the level of water in the flume, an acrylic smooth plate, transparent and 0.5 inches thick, is positioned parallel to the bed of the flume (shown in Figure 8). The smooth plate measures 1.5×1.1 m, supported by six legs with adjustable lengths. These legs are affixed to the original bed of the flume. A new turbulent boundary layer was formed on the suspended smooth plate placed inside the channel. The smooth plate was located 8 m from the channel inlet and the cylinder was mounted 0.7 m measured from the beginning of the plate. The flow depth (H) is 85 mm. The flow characteristics were studied using $Re = 1.45 \times 10^4$ based on cylinder diameter. The overall uncertainty of the PIV measurements at a 95% confidence interval for the mean streamwise velocity, Reynolds normal stress, and Reynolds shear stress was 2%, 6%, and 4%, respectively. The approach flow conditions, and the measurement uncertainty analysis are the same as that used by Thakurta and Balachandar (2025) and not repeated here for brevity.

Various circular cylinders with and without passive modifications, including PC, SC, CSC, CWH, HSC, FC, and MC, were investigated at emergent condition (shown in Figure 2). Table 6 shows the parameters used for various cylinder types in current experimental studies. The flow velocity measurements were carried out using a planar PIV system. To capture the variation of velocity

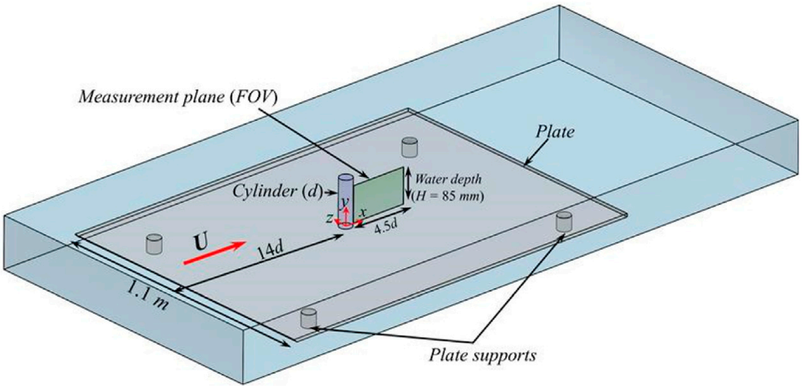

FIGURE 8
Measurement plane used in the current experimental setup.

TABLE 6 Parameters used for various cylinder types in current experimental studies. Nomenclature: *d* = cylinder diameter, SC = single-slotted cylinder, CSC = cross-slotted cylinder, HSC = helical straked cylinder, MC = meshed cylinder, CWH = cylinder with holes, and FC = foam-covered cylinder.

Parameter [range from literature review]	SC	CSC	HSC	MC	CWH	FC
Flow incidence angle, θ [0°–90°]	0°	0°	0°	0°	0°	0°
Slot size, s/d [0.016–0.400]	0.1	0.1	–	–	–	–
Number of helix, n [1–4]	–	–	3	9	–	–
Strake pitch, p/d [3–20]	–	–	10	2	–	–
Strake height, h/d [0.05–0.30]	–	–	0.2	0.02	–	–
Diameter ratio, d_h/d [0.005–0.200]	–	–	–	–	0.1	–
Hole-to-hole gap ratio, s_h/d [0.1–1.4]	–	–	–	–	0.4	–
Porosity, $1 - \varnothing$ [0.629–0.999]	–	–	–	–	–	0.95

along the flow depth, the field-of-view (FOV) in the vertical midplane (x-y plane) was chosen (shown in Figure 8). The system included dual pulse Nd:YAG lasers (Litron Nano PIV Laser) with a wavelength of 532 nm and 120 mJ/pulse energy. Cylindrical lenses with focal lengths of 15 mm and 25 mm were used to generate a laser sheet of around 2 mm. PIV images from two PowerViewPlus 8 MP CCD cameras with a resolution 3312 × 2488 pixels were acquired simultaneously to capture the streamwise vertical FOV after the cylinder. The cameras are equipped with Nikon AF NIKKOR 50 mm lenses with the frequency of 2.42 Hz. The glass spheres with silver coating and 1,100 kg/m^3 density are used as seeding particles. A total of 2,000 image pairs were captured for each experiment.

PIV images were processed using open-source PIVlab software (Thielicke and Stamhuis, 2014). Initial background subtraction was followed by the contrast-limited adaptive histogram equalization (CLAHE) technique (Pizer et al., 1987). The image pairs were correlated using the Fast Fourier Transform window deformation algorithm. The image analysis occurred in two stages: initially, using 64 × 64 pixels window, which was then downsized to a smaller 32 × 32 pixels interrogation size in the second stage, with a spatial overlap of 50%. The final process yielded an interrogation size of 16 × 16 pixels. After completing the image analysis, the data was post-processed by applying median filters. The local median outlier detection method proposed by Westerweel and Scarano (Pizer et al., 1987) was applied to identify and remove erroneous vectors. Fewer than 5% of the vectors were flagged as spurious and subsequently replaced with interpolated values. The final velocity field of each FOV consists of 31,724 uniformly spaced vectors with a spatial resolution of the data dependent on the size of the FOV. Mean velocity and turbulence quantities were then computed using a developed code.

4 Results and discussion

Figure 9 shows the contour plots of the mean streamwise velocity (U/Um, where U_m is the mean velocity prior to any cylinder installation) in the central vertical plane ($z/d = 0$), overlaid with the streamtraces of mean velocity for various configurations of wall-mounted cylinders. Figure 9a highlights a prominent counterclockwise recirculation region behind the plain cylinder (PC), centered at $x/d = 0.85$ and $y/H = 0.30$. This recirculation region arises due to the strong upwash flow induced by the base vortices from the bed into the wake region. The upwash extends the flow behind the cylinder across the entire water depth until it reaches the free surface. The flow then moves toward the cylinder, rolls up due to its presence, and eventually returns toward

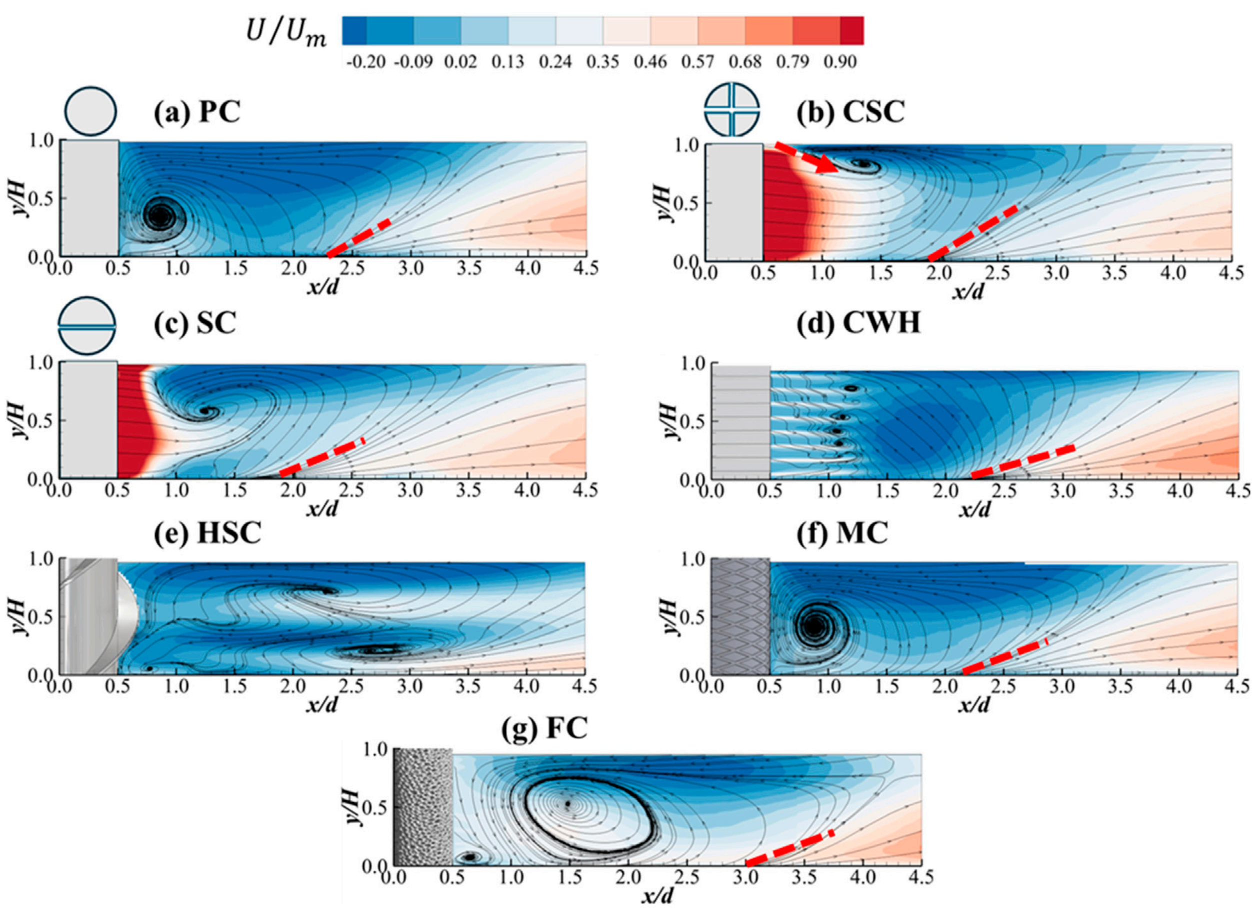

FIGURE 9
Comparison of mean normalized streamwise velocity contours superimposed with velocity streamlines in the vertical mid plane. Nomenclature: d = cylinder diameter, U_m = mean velocity, PC = plain cylinder, SC = single-slotted cylinder, CSC = cross-slotted cylinder, HSC = helical straked cylinder, MC = meshed cylinder, CWH = cylinder with holes, and FC = foam-covered cylinder. **(a)** PC, **(b)** CSC, **(c)** SC, **(d)** CWH, **(e)** HSC, **(f)** MC, **(g)** FC.

the bed, forming the recirculation region. At x/d = 2.3, the flow bifurcates into forward and backward flow regions, marked by the red dashed line in Figure 9a. The backward flow feeds the recirculation zone, while the forward flow moves downstream. Figure 9a will serve as a base case to compare with the rest of the configurations.

The velocity contour for the cross-slotted cylinder (CSC), shown in Figure 9b, exhibits a markedly different trend compared to PC in Figure 9a. A region of high magnitude of mean streamwise velocity (U/Um) is observed within the region $0.5 \le x/d \le 1.0$, due to the high-velocity jet exiting from the slot. This high-velocity region is present through most of the water depth, except near the free surface. The jet also shifts the center of the recirculation region farther downstream and closer to the free surface, at x/d = 1.35 and y/H = 0.80. Flow past a circular cylinder typically involves flow separation induced by an adverse pressure gradient along the cylinder surface, with the separation point depending on *Re*. However, in general the cross-slot fixes the separation point along the cylinder surface at the location of the slot due to the sharp edge. The turbulent motions generated by this controlled separation may contain higher energy, leading to noticeable deformation of the free surface. This explains the absence of a high-velocity region and the presence of downwash flow (indicated by the red dashed arrow in Figure 9b) near the free surface. Additionally, the bifurcation represented by the red dashed line is closer to the cylinder near the bed (x/d = 1.9) compared to PC, due to the high-velocity jet promoting forward flow.

A similar trend is observed for the single-slotted cylinder (SC) in Figure 9c. A region of high magnitude of mean streamwise velocity (U/Um) is observed within the region $0.5 \le x/d \le 0.8$, due to the high-velocity jet exiting from the slot. However, the high-velocity jet region is shorter and spans the entire water depth, suggesting less prominent surface deformation compared to the CSC. It should be noted here that the flow separation points in the case of SC will be controlled by the flow *Re*. The jet also shifts the center of the recirculation region downwards from the free surface, at x/d = 1.2 and y/H = 0.6.

For the cylinder with holes (CWH) in Figure 9d, six distinct spiraling flow regions are observed, resulting from the interaction of the positive velocity issuing from the holes with the downward velocity in the wake region. It should be noted that the jets near the free surface and the bed do not have distinct spiraling flows. The streamwise velocity contour for the CWH indicates that the flow through the holes is less intense than the jet flow from the slots in the CSC and SC cases (Figures 9b,c). Furthermore, the flow bifurcation point shifts downstream to x/d = 2.2, similar to the PC case.

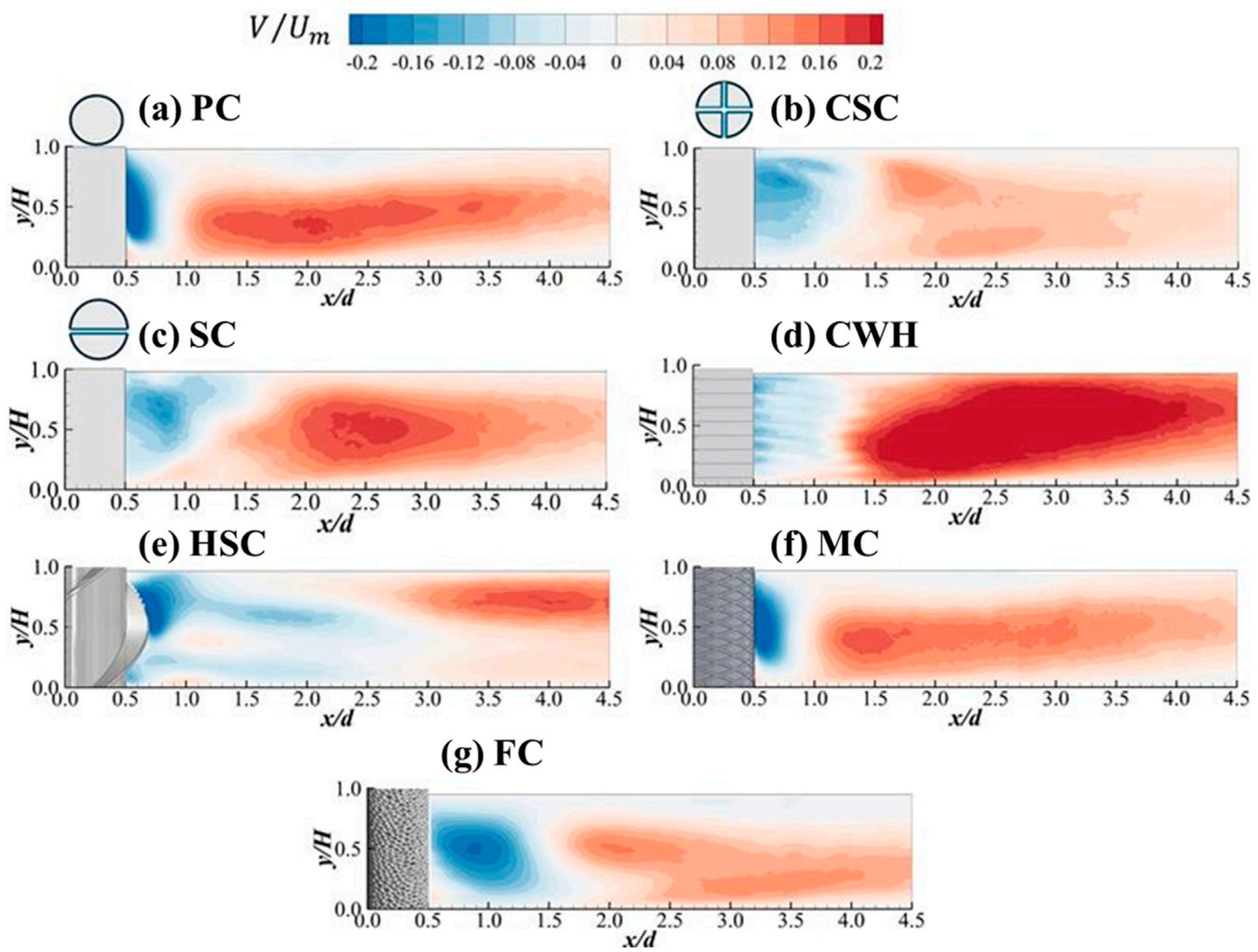

FIGURE 10
Comparison of mean normalized vertical velocity contours superimposed with velocity streamlines in the vertical mid plane. **(a)** PC, **(b)** CSC, **(c)** SC, **(d)** CWH, **(e)** HSC, **(f)** MC, **(g)** FC.

In the case of the helical straked cylinder (HSC) in Figure 9e, the wake flow is guided by the helical strakes, confined by the bed and the free surface, resulting in three distinct focal points indicated by spiraling stream traces centered at $y/H = 0.05$, 0.20, and 0.70. Unlike PC, where the stream traces roll up to form a recirculation region, the flow in the HSC is guided downward by the strakes, inducing a channelized flow. Additionally, the stream traces reveal a saddle point at $x/d = 3.0$ and $y/H = 0.4$, attributed to flow separation at various angles caused by the helical strakes. Notably, the bifurcation point on the bed is absent in the HSC. A flow pattern similar to that of the PC (Figure 9a) is observed for the mesh cylinder (MC) in Figure 9f. However, the center of the recirculation region is located at $y/H = 0.4$, slightly higher than that for the PC. The similarity in streamwise velocity and flow patterns between the PC and MC indicates that the mesh has minimal impact on the wake flow dynamics.

For the foam-covered cylinder (FC) in Figure 9g, two distinct recirculation regions are observed: a primary recirculation region located at $x/d \approx 1.5$ and $y/H \approx 0.5$, and a secondary recirculation region at $x/d \approx 0.6$ and $y/H \approx 0.1$, with the former being significantly larger. The secondary recirculation forms as a result of the interaction between the upwash induced by the base vortices and the downward flow along the cylinder surface, producing spiraling stream traces near the wake centerline. The primary recirculation region is displaced farther downstream due to bleed flow through the porous foam, which delays shear layer roll-up and leads to an expanded and more diffused wake.

Figure 10 shows the contour of mean vertical velocity (V/U_m) in the central vertical plane ($z/d = 0$). Figure 10a for PC serves as the baseline with no modifications. A region of negative (downward) vertical velocity can be observed behind the cylinder ($x/d \approx 0.50-0.75$ and $y/H \approx 0.2-1.0$), which relates to the strong downflow of the recirculation region. However, in the region $y/H < 0.2$, a region of positive (upward) vertical velocity is observed close to the bed. This is attributed to the upwash of the base vortices from the bed into the wake region, as mentioned earlier in Figure 9a. Beyond $x/d \approx 1.0$, the upwash flow induces a positive (upward) vertical motion of the fluid that extends across the entire water depth with vertical distribution varying along the streamwise direction. The strongest vertical velocities appear near $x/d \approx 0.5$–0.75 (downward) and around $x/d = 2$ (upward).

For the CSC case, Figure 10b, incorporating two perpendicular slots significantly alters the vertical velocity field in the wake. Primarily, the region of negative velocity behind the cylinder is significantly larger than PC, however, the magnitude is comparatively lower due to the jet issuing from the slot. The strong streamwise velocity from the slot weakens the roll-up of the streamlines behind the cylinder, as observed in the case of PC, thus weakening the downward flow along the cylinder. Furthermore, the magnitude of V/Um after $x/d = 1.5$ appears lower than as observed in PC. This is due to the blowing/suction effect from the slot perpendicular to the flow direction and has been reported by Boamah (Boamah, 2024) for a single-slotted cylinder with the slot normal to the flow direction. Overall, the CSC configuration stabilizes the wake and promotes nearly uniform flow with lower vertical motion.

In case of SC, Figure 10c, with one parallel slot, the wake's vertical velocity field is altered, though less dramatically than in the CSC case. The magnitude of the upward flow after $x/d = 1.5$ is comparatively higher than CSC. As observed in the streamwise velocity contour plot in Figure 9c, the high-velocity jet exiting the slot has a shorter span compared to CSC in Figure 9b. As a result, the stream traces spiral closer to the cylinder in SC than in CSC, leading to a much stronger upward flow motion in SC.

Figure 10d shows the mean vertical velocity contours for CWH. Similar to the slotted cases, the holes allow fluid to bleed through the back, weakening vortex development. The V/U_m field shows weak and localized vertical motions in the near-wake region ($x/d \approx 0.5$–1.2) that dissipate rapidly downstream. This behavior reflects the influence of hole-induced spiral flows, which also appear in the streamwise contours (Figure 9d). However, beyond $x/d = 1.5$, a region of upward flow emerges with increasing intensity, more pronounced than in other passive control cases.

In Figure 10e, unlike the slotted configurations, the HSC uses external strakes to modify the flow field. These helical strakes generate secondary, spiraling flow structures that disrupt coherent vortex shedding and induce helical motion in the wake. The region of negative V/U_m extends downstream up to $x/d \approx 2.5$. Beyond $x/d = 3.0$, a strong upward flow develops in the upper half of the wake ($y/H > 0.5$), corresponding to spiraling streamlines that converge near $y/d \approx 2.40$, as observed in the streamwise velocity plots.

For the case of MS, Figure 10f, the flow pattern is similar to that of PC case, which further supports the minimal impact of the mesh on the wake flow dynamics as highlighted previously. In case of FC, Figure 10g, the negative velocity region ($x/d \approx 0.5$–1.5) behind the cylinder has a significantly larger size as compared to PC. This observation aligns with the larger primary recirculation region observed behind the cylinder, which is located further away from the cylinder as compared to PC.

While the velocity contour plots provided an overall view of the flow field features behind different cylinder configurations, analyzing velocity profiles at various streamwise locations is essential to gain more insights into these effects. These profiles offer a more detailed perspective on the distribution and variation of flow velocity in the wake. Figures 11a,b present the distribution of the mean streamwise velocity (U/U_m) profile along the water depth (H) at $x/d = 0.75$ and $x/d = 2.50$, respectively. At $x/d = 0.75$, the PC exhibits negative velocity above $y/H = 0.30$, corresponding to the large recirculation region observed in the contour plot of Figure 9a. Similarly, MC displays a comparable magnitude of streamwise velocity. In contrast, for CSC and SC, the velocity is predominantly positive and significantly higher, especially for the CSC, which can be attributed to the high jet velocity from the slot.

The velocity profiles for the CWH show a markedly different trend, with distinct peaks aligned with the high-velocity regions issuing from the holes, as observed in Figure 9d. For the foam cylinder (FC), at $x/d = 0.75$ (Figure 11a), the velocity remains relatively steady with minimal variation for $y/H > 0.18$. However, near the bed ($y/H < 0.18$), the profile exhibits negative velocity. In the case of HSC, the U/U_m values remain predominantly negative across the water depth, except within $0.50 \le y/H \le 0.65$, where they are positive. The meandering shape of the HSC profile reflects the helical configuration of the strakes.

Further downstream at $x/d = 2.50$ (Figure 11b), the velocity profiles for all cylinder configurations, except the HSC, show similar trends. Additionally, differences in U/U_m values are less prominent compared to those at $x/d = 0.75$, suggesting a diminishing influence of the cylinder's geometric modifications farther downstream. However, for the HSC, the meandering velocity profile observed at $x/d = 0.75$ becomes even more pronounced at $x/d = 2.50$, highlighting the persistent influence of the strakes in the far wake.

Figures 11c,d illustrate the root mean squared streamwise velocity (u_{rms}/U_m) profiles along the water depth at $x/d = 0.75$ and $x/d = 2.50$, respectively. Similar to the mean velocity profiles, the CSC and the SC exhibit higher u_{rms} values due to the elevated streamwise velocity fluctuations (u') induced by the jet flow through the slot. For the CWH, the u_{rms} profiles display distinct peaks resulting from the interaction between the flow through the holes and the wake region. Notably, the peak magnitudes of u_{rms} for the CWH exceed those for the CSC and, in some regions, the SC. This suggests that the holes locally enhance streamwise turbulence levels near their locations.

The u_{rms} values for the HSC are similar to those for the PC and the MC, while the FC demonstrates a lower level of streamwise turbulence across the water depth. At $x/d = 2.50$, however, the trend reverses, with the PC and the MC exhibiting higher streamwise turbulence levels than the CSC, the SC, and the CWH. The HSC again displays a unique pattern, with significant variations in the u_{rms} profile across the water depth. These variations correspond to regions of intense turbulence caused by interactions between the multiple separated shear layers, as discussed earlier.

Figure 12 shows the contours of the root mean squared streamwise velocity (u_{rms}/U_m) in the near wake for each cylinder configuration. Figure 12a shows a lower magnitude of u_{rms} behind the PC, which gradually increases downstream beyond $x/d = 1.0$. For the CSC and SC cases, shown in Figures 12b,c, the maximum magnitude of u_{rms} occurs directly behind the cylinder due to the interaction between the counterclockwise recirculation zone and the high-velocity jet flow exiting the slot. The intensity of u_{rms} decreases progressively downstream ($x/d > 1.5$), indicating that streamwise velocity fluctuations (u') are relatively suppressed in the downstream region.

In the case of the CWH, shown in Figure 12d, high levels of u_{rms} are observed in the region $0.5 \le x/d \le 1.5$, resulting from the interaction between the flow through the holes and the wake region. Beyond $x/d = 1.5$, the magnitude of u_{rms} decreases to levels similar to those observed for the PC in Figure 12a. This suggests that the jet flow through the holes has a limited influence on increasing turbulence in the wake region. For the HSC, shown in

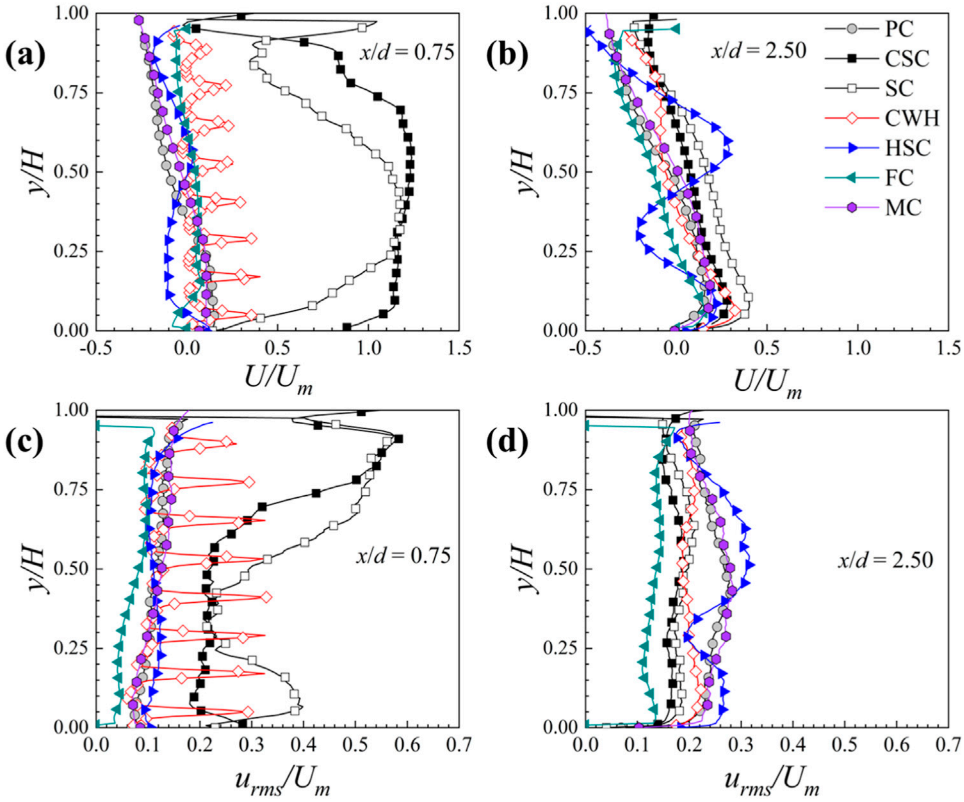

FIGURE 11
Comparison of mean normalized streamwise velocity and normalized turbulent kinetic energy profiles at different streamwise locations in the vertical mid plane. **(a)** U/U_m at x/d = 0.75, **(b)** U/U_m at x/d = 2.50, **(c)** u_{rms}/U_m at x/d = 0.75, **(d)** u_{rms}/U_m at x/d = 2.50.

Figure 12e, a high level of turbulence is generated due to the interaction of multiple separated shear layers caused by the strakes. Notably, two regions of elevated u_{rms} are identified: one near the bed at x/d = 2.5 and y/H = 0.1, and another at x/d = 2.5 and y/H = 0.6. Finally, for the MC case shown in Figure 12f, the contours of u_{rms} closely resemble those of the PC in Figure 10a. This confirms that the presence of the mesh has a minimal impact on the flow characteristics in the wake region.

In the case of FC, the contours of u_{rms} in Figure 12g shows a much lower magnitude compared to PC case indicating reduced velocity gradients and lesser fluctuations. This suggests that a foam covering can serve as a protective layer by disrupting large-scale flow structures, thereby shielding the cylinder from vortex shedding-induced oscillations. Similarly, foam covering may also help mitigate downstream scouring around bridge piers or comparable hydraulic structures.

To better understand the flow field dynamics for each cylinder configuration, instantaneous contours of the normalized streamwise velocity (u/U_m) are presented in Figure 13. Although each snapshot represents an independent moment in time (i.e., they are not temporally correlated), together they illustrate the spatial behavior and variability of wake flow structures. Each contour plot is also overlaid with instantaneous velocity vectors to aid in interpretation.

The PC case, depicted in Figure 13a, shows that its wake is predominantly characterized by positive streamwise velocity across the cylinder height, except near the free surface (approximately y/H > 0.7) where a region of reversed (negative) velocity appears. This surface-level negative-velocity region is concentrated just below the free surface and extends downstream to about $x/d \approx 3.0$, beyond which the streamwise flow returns to positive values. A similar pattern is observed in the second snapshot, though in that instance the negative-velocity region persists over a larger portion of the cylinder height. Both snapshots reveal a strong positive velocity region near the bed (y/H < 0.3), attributed to the upward motion induced by the base vortices.

The CSC produces a strong jet of streamwise flow through its slots, resulting in a region of high positive velocity in the wake (Figure 13b). However, the jet's distribution along the height varies with time. In the first snapshot, the jet is stronger in the lower half (y/H < 0.5), whereas in the second snapshot it is more pronounced in the upper half (y/H > 0.5). This alternating jet behavior suggests a dynamic flow mechanism likely driven by the orthogonal slot configuration's alternating suction-and-blowing effect. Such a mechanism enhances mixing in the wake and could be advantageous for heat transfer applications. In both snapshots for the CSC, any region of negative streamwise velocity is greatly diminished and remains confined near the free surface, consistent with the smaller recirculation zones observed in the time-averaged flow field for this configuration.

In the SC case (Figure 13c), the longitudinal slot produces a jet that also exhibits temporal variation. In the first snapshot, the jet

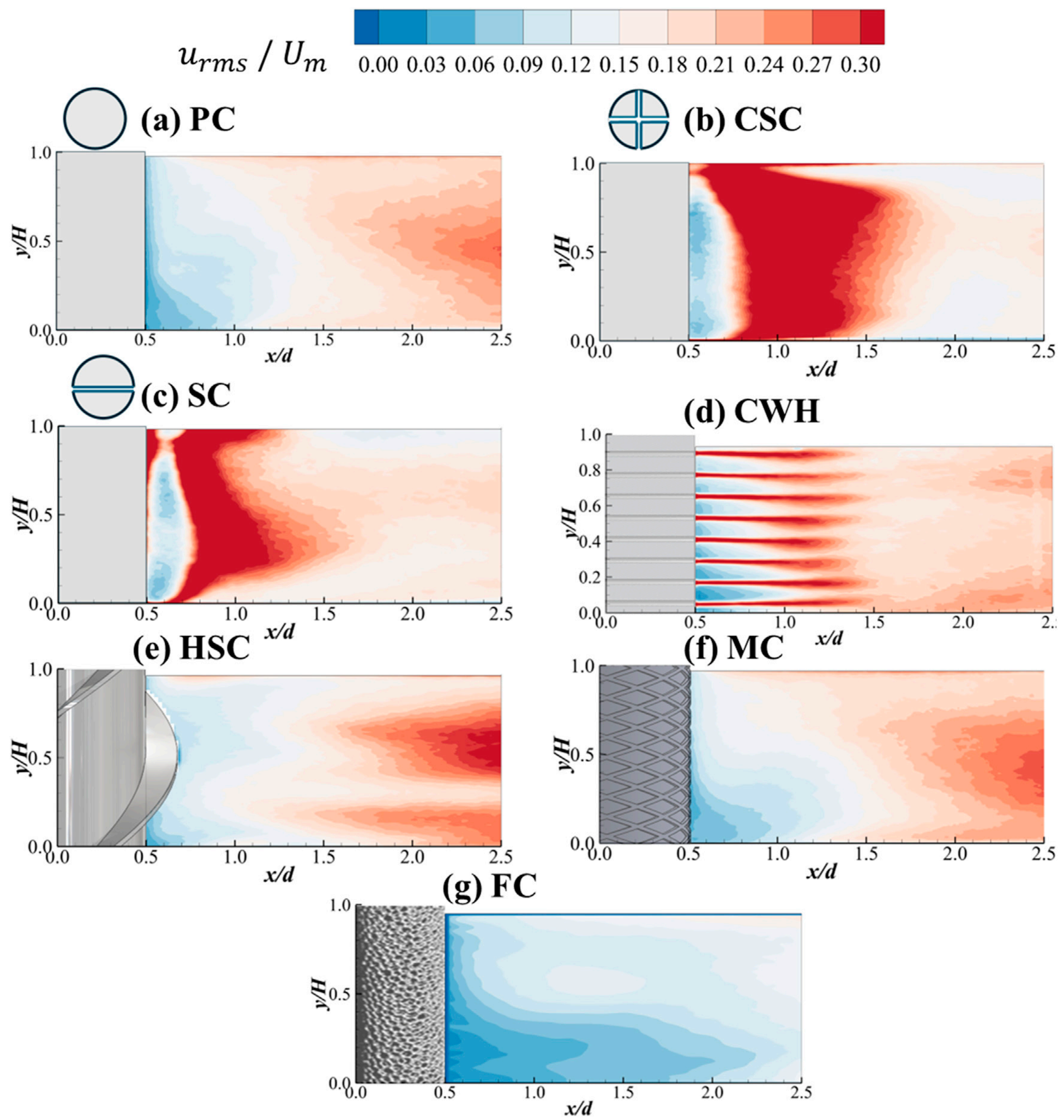

FIGURE 12
Comparison of mean normalized root mean squared streamwise velocity contours in the vertical mid plane. **(a)** PC, **(b)** CSC, **(c)** SC, **(d)** CWH, **(e)** HSC, **(f)** MC, **(g)** FC.

extends farther downstream into the wake, whereas in the second instance it is shorter and more tightly confined near the cylinder. These differences imply a pulsating or "pumping" behavior of the jet, likely due to unsteady shear layer interactions at the slot opening.

For the CWH case, Figure 13d, the wake is marked by multiple high-velocity streaks (jets) emerging from the holes in the cylinder wall. In the first snapshot, these hole-induced jets are clearly visible, extending downstream to about $x/d = 1.5$ and appearing relatively uniform along the height. In contrast, the other instance shows that the jet strength diminishes near both the bed ($y/H < 0.2$) and the free surface ($y/H > 0.8$), indicating greater variability along the height. Beyond $x/d \approx 1.5$, a region of negative streamwise velocity develops, suggesting that the influence of the hole-induced jets is mostly confined to the near-wake region. This transient, highly localized jet behavior can be beneficial in near wake flow control applications like heat transfer enhancement.

The HSC, Figure 13e, exhibits instantaneous flow structures that are not evident in the time-averaged results. These features—originating from unsteady shear layers shed at the tips of the strakes—act as localized disturbances in the wake, and their position and intensity vary between the two snapshots. Their irregular and intermittent appearance suggests that the strakes introduce wake instabilities which evolve and dissipate dynamically. Consequently, the HSC produces a more complex and unsteady wake field compared to the other configurations, even though these transient structures cancel out in the mean flow. Such unsteady flow behavior, characterized by frequent vortex interactions and enhanced mixing, can be beneficial for

10.3389/fmech.2025.1595832

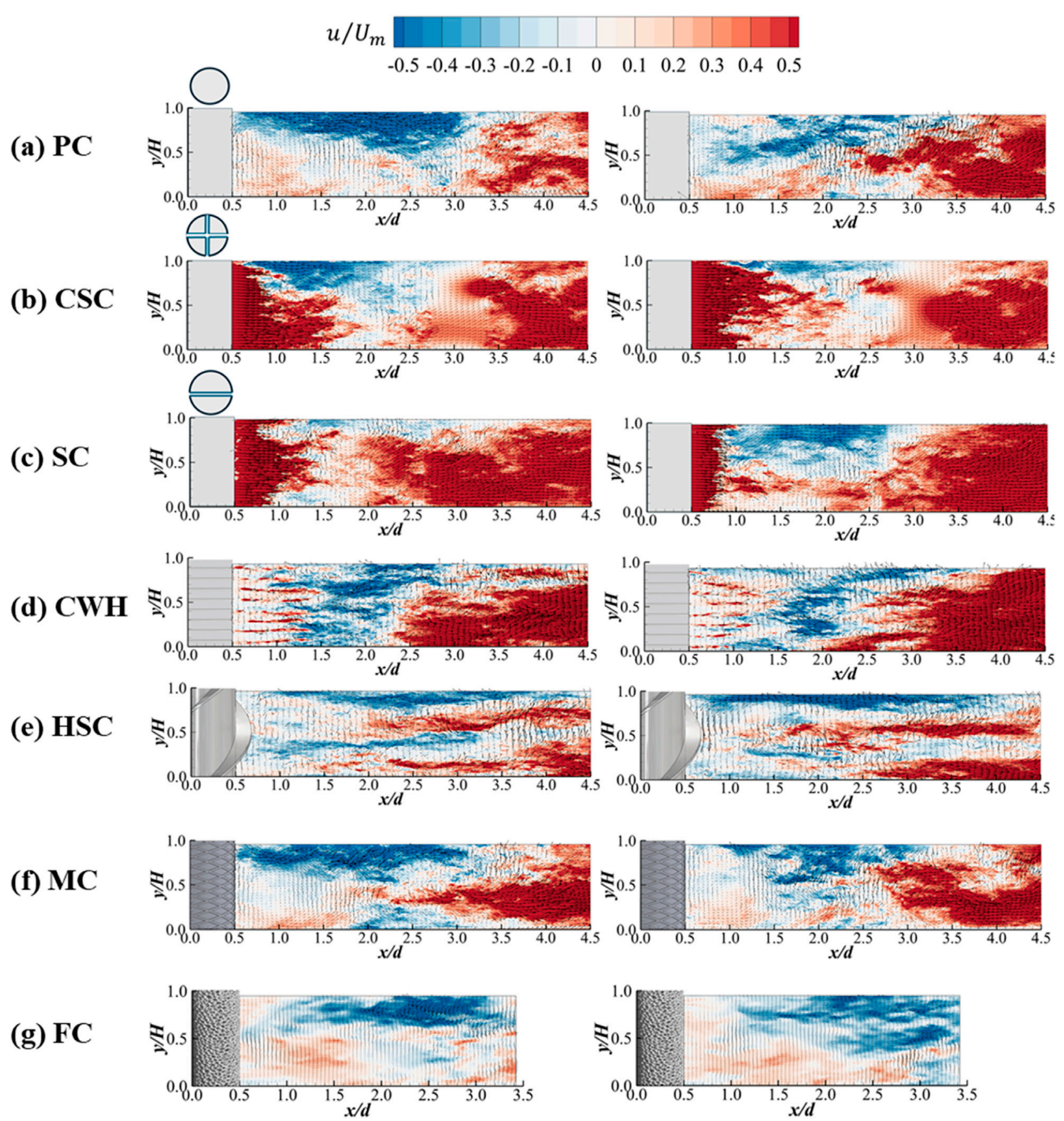

FIGURE 13
Comparison of instantaneous flow field at two instances in the vertical mid plane. **(a)** PC, **(b)** CSC, **(c)** SC, **(d)** CWH, **(e)** HSC, **(f)** MC, **(g)** FC.

wake-induced heat transfer enhancement, particularly in applications where increased turbulence promotes improved convective performance. Whereas the MC case (shown in Figure 13f) shows instantaneous flow patterns very similar to those of the PC. No significant unique flow structures were observed in the MC case beyond what was described for the PC.

Lastly, the FC, Figure 13g, has a porous surface which allows some bleed-through of flow. This results in a region of positive streamwise velocity maintained close to the cylinder surface in the instantaneous snapshots, although its magnitude is lower than that observed for the CSC, SC, or CWH configurations. The region of negative streamwise velocity remains consistently confined near the free surface ($y/H > 0.5$) in both instances, indicating a relatively stable wake for the FC. This steady, restrained wake pattern is also reflected in the time-averaged results (Figure 9g), confirming that the foam-covered cylinder configuration produces a less dynamic and less fluctuating flow field compared to the other modified cylinders.

5 Conclusions and future recommendations

This study provides a comprehensive review of passive flow control mechanisms in flow past bed-mounted circular cylinders, including helical strakes, meshes, foam coverings, slots, and holes, highlighting their principles, applications, and effects. Existing experimental and numerical studies reveal a lack of comparative analyses and inconsistencies in the approach flow conditions of various flow control methods. To address this gap, particle image velocimetry measurements were conducted at a Reynolds number of 1.45×10^4 to evaluate wake flow characteristics under identical or near-identical inflow conditions. The following conclusions are drawn from this research:

- For the plain cylinder, the wake flow is dominated by a large counterclockwise recirculation region induced by upwash from the bed. This results in negative velocities near the bed and a bifurcation point downstream.
- The cross-slotted cylinder and single-slotted cylinder introduce high-velocity jets in the wake region, significantly altering the flow structure. These jets shift the recirculation region upward and downstream, fix the flow separation points, and enhance turbulence intensity near the cylinder. Notably, the cross-slotted cylinder exhibits the highest velocity and turbulence in the near wake compared to the other cases, highlighting its potential for applications involving drag reduction and heat transfer enhancement. Moreover, it offers a weight reduction advantage compared to the helical straked cylinder.
- The cylinder with holes exhibits distinct spiraling flow regions and localized turbulence peaks due to interactions between flow through the holes and the wake region. However, the turbulence effect diminishes downstream.
- The helical straked cylinder demonstrates unique flow behavior, with the strakes guiding the wake flow and generating multiple focal points and channelized flow patterns. Unlike other configurations, the helical straked cylinder maintains pronounced meandering velocity profiles and high turbulence levels downstream, indicating a persistent influence of the strakes even in the far wake. However, the extra material added to the cylinder results in an increase in the overall weight of the system.
- The meshed cylinder exhibits minimal deviation from the flow characteristics of the plain cylinder, confirming the limited impact of the mesh on the wake flow.
- The foam-covered cylinder dampens flow fluctuations and reduces turbulence across the water depth, making it suitable for applications requiring flow stability and drag mitigation.

The current study provided an extensive review of individual passive flow control methods and addressed the gap in the lack of comparative studies evaluating the effectiveness of various techniques under similar flow conditions. To address the identified limitations of passive flow control mechanisms, the following recommendations are proposed for future research.

- Detailed numerical and experimental investigations are required to evaluate the influence of critical parameters such as flow incidence angles, Reynolds number, and slot spacing-to-diameter ratio for cross-slot configurations. This level of analysis is necessary to extend the understanding developed for single-slot cases to more complex configurations.
- While some experimental work has been conducted on cylinders with holes, a comprehensive numerical investigation of the flow field is lacking. Future research can be focused on high fidelity numerical simulations to gain further understanding into wake dynamics, turbulence modulation, and flow separation mechanisms associated with this configuration.
- Although helical strakes have been widely recognized for their effectiveness in mitigating vortex-induced vibrations, their influence on heat transfer rates remains unexplored. Future studies can be conducted on understanding the impact of the vortical structures induced by helical strakes on heat transfer rates.
- While this study presents a comprehensive experimental comparison of passive flow control strategies through detailed flow field analysis, future research should extend these findings by incorporating high-fidelity numerical simulations and directly investigating the effects on vortex-induced vibrations and convective heat transfer. Such complementary computational investigations would provide deeper insights into three-dimensional flow structures, pressure fields, and turbulence characteristics, thereby enhancing the overall understanding and applicability of these flow control techniques across diverse engineering scenarios.

Data availability statement

The raw data supporting the conclusions of this article will be made available by the authors, without undue reservation.

Author contributions

ZT: Data curation, Formal Analysis, Investigation, Methodology, Validation, Visualization, Writing – original draft, Writing – review and editing. SB: Formal Analysis, Investigation, Validation, Visualization, Writing – original draft. RB: Conceptualization, Funding acquisition, Investigation, Methodology, Project administration, Resources, Supervision, Validation, Visualization, Writing – review and editing.

Funding

The author(s) declare that financial support was received for the research and/or publication of this article. The authors acknowledge the support of the Natural Sciences and Engineering Research

Council of Canada (NSERC) for funding this project under the Discovery Grant program.

Acknowledgments

The authors gratefully acknowledge the contributions of the Thermofluids Research Group at the University of Windsor. Shinneeb and Maria Gudisey provided the particle image velocimetry measurement data for cylinders with foam covering and holes, respectively. The results for single-slotted and helical straked cylinders were provided by Boamah and Thakurta, respectively. The authors also thank Roussinova for providing Figure 1.

Conflict of interest

The authors declare that the research was conducted in the absence of any commercial or financial relationships that could be construed as a potential conflict of interest.

The author(s) declared that they were an editorial board member of Frontiers, at the time of submission. This had no impact on the peer review process and the final decision.

Generative AI statement

The author(s) declare that no Generative AI was used in the creation of this manuscript.

Publisher's note

All claims expressed in this article are solely those of the authors and do not necessarily represent those of their affiliated organizations, or those of the publisher, the editors and the reviewers. Any product that may be evaluated in this article, or claim that may be made by its manufacturer, is not guaranteed or endorsed by the publisher.

References

Abdollahzadeh Jamalabadi, M. Y. (2021). Active and passive control of a galloping cylinder with heat transfer. *J. Therm. Analysis Calorim.* 145, 1827–1835. doi:10.1007/s10973-020-10385-8

Ain, Q. U., Khan, Y., Mahmood, R., Alameer, A., Majeed, A. H., and Faraz, N. (2022). Passive control of hydrodynamic forces on a circular obstacle in a transient flow: FEM computations. *Front. Phys.* 10, 928087. doi:10.3389/fphy.2022.928087

Akilli, H., and Rockwell, D. (2002). Vortex formation from a cylinder in shallow water. *Phys. Fluids* 14 (9), 2957–2967. doi:10.1063/1.1483307

Alhashem, A., Alshareef, S., Alharbi, A. Y., and Alrahmani, M. A. (2024). Fluid dynamic and thermal performance of a V-shape slotted cylinder. *Energies* 17 (23), 6192. doi:10.3390/en17236192

Ali, U., Islam, M., Janajreh, I., Fatt, Y., and Alam, M. M. (2021). Flow-induced vibrations of single and multiple heated circular cylinders: a review. *Energies* 14 (24), 8496. doi:10.3390/en14248496

Alshareef, S., Harman, T., and Ameel, T. (2022). "Thermal fluid assessment of cylinders with multiple slots in aligned flow," in *21st IEEE Intersociety Conference on thermal and Thermomechanical Phenomena in electronic systems (iTherm)*, 1–9.

Arbak, A., and Dukhan, N. (2020). Performance and heat transfer measurements in asymmetrically heated metal foam cooled by water. *Therm. Sci. Eng. Prog.* 20, 100688. doi:10.1016/j.tsep.2020.100688

Arcondoulis, E. J., Liu, Y., Li, Z., Yang, Y., and Wang, Y. (2019). Structured porous material design for passive flow and noise control of cylinders in uniform flow. *Materials* 12 (18), 2905. doi:10.3390/ma12182905

Ashtiani Abdi, I., Khashehchi, M., and Hooman, K. (2017). Investigation of coherence behind a single foamed tube. *Fluid Mech. Res. Int. J.* 1 (2), 45–54. doi:10.15406/fmrij.2017.01.00007

Ashtiani Abdi, I., Khashehchi, M., and Modirshanechi, M. (2014). "A comparative analysis on the velocity profile and vortex shedding of heated foamed cylinders," in *19th Australasian fluid mechanics Conference* (Australia: Australasian Fluid Mechanics Society).

Baek, H., and Karniadakis, G. E. (2009). Suppressing vortex-induced vibrations via passive means. *J. Fluids Struct.* 25 (5), 848–866. doi:10.1016/j.jfluidstructs.2009.02.006

Balachandar, R., Ramachandran, S., and Tachie, M. F. (2000). Characteristics of shallow turbulent near wakes at low Reynolds numbers. *J. Fluids Eng.* 122 (2), 302–308. doi:10.1115/1.483258

Balachandar, R., Tachie, M. F., and Chu, V. H. (1999). Concentration profiles in shallow turbulent wakes. *Trans. ASME J. Fluids Eng.* 121, 34–43. doi:10.1115/1.2822007

Bao, Z., Qin, G., He, W., and Wang, Y. (2018). Numerical investigation of flow around a slotted circular cylinder at low Reynolds number. *J. Wind Eng. Ind. Aerodyn.* 183, 273–282. doi:10.1016/j.jweia.2018.11.010

Barman, J., and Kumar, B. (2022). Turbulence in a compound channel with the combination of submerged and emergent vegetation. *Phy. Fluid* 34 (4). doi:10.1063/5.0086739

Bhattacharyya, S., Dhinakaran, S., and Khalili, A. (2006). Fluid motion around and through a porous cylinder. *Chem. Eng. Sci.* 61 (13), 4451–4461. doi:10.1016/j.ces.2006.02.012

Bhattacharyya, S., and Singh, A. K. (2011). Reduction in drag and vortex shedding frequency through porous sheath around a circular cylinder. *Int. J. Numer. Methods Fluids* 65 (6), 683–698. doi:10.1002/fld.2210

Boamah, J. (2024). *Effect of incidence angle on the wake flow of a wall-mounted cylinder with a slot immersed in a shallow flow*. Canada: University of Windsor. Master's thesis.

Boules, D., Sharqawy, M. H., and Ahmed, W. H. (2021). Enhancement of heat transfer from a horizontal cylinder wrapped with whole and segmented layers of metal foam. *Int. J. Heat. Mass Transf.* 165, 120675. doi:10.1016/j.ijheatmasstransfer.2020.120675

Bruneau, C. H., and Mortazavi, I. (2008). Numerical modelling and passive flow control using porous media. *Comput. Fluids* 37, 488–498. doi:10.1016/j.compfluid.2007.07.001

Carmo, B. S., Gioria, R. S., Korkischko, I., Freire, C. M., and Meneghini, J. R. (2012). Two-and three-dimensional simulations of the flow around a cylinder fitted with strakes. *Int. Conf. Offshore Mech. Arct. Eng.* 44922, 781–790. doi:10.1115/omae2012-83603

Chang, W. Y., Constantinescu, G., and Tsai, W. F. (2017). On the flow and coherent structures generated by a circular array of rigid emerged cylinders placed in an open channel with flat and deformed bed. *J. Fluid Mech.* 831, 1–40. doi:10.1017/jfm.2017.558

Chatelain, M., and Proust, S. (2021). Open-channel flows through emergent rigid vegetation: effects of bed roughness and shallowness on the flow structure and surface waves. *Phy. Fluid* 33 (10). doi:10.1063/5.0063288

Chen, D., and Jirka, G. H. (1995). Experimental study of plane turbulent wakes in a shallow water layer. *Fluid Dyn. Res.* 16 (1), 11–41. doi:10.1016/0169-5983(95)00053-g

Chen, D. Y., Abbas, L. K., Wang, G. P., Rui, X. T., and Lu, W. J. (2019). Suppression of vortex-induced vibrations of a flexible riser by adding helical strakes. *J. Hydr.* 31 (3), 622–631. doi:10.1007/s42241-018-0078-6

Chen, G., Shahsavari, A., Hosseini, S., Kim, S., Chen, W. L., and Kim, K. C. (2023). Wake flow evolution behind a circular cylinder with two perpendicular slits at various angles of attack. *J. Vis.* 26 (6), 1233–1246. doi:10.1007/s12650-023-00934-2

Chen, W. L., Huang, Y., Chen, C., Yu, H., and Gao, D. (2022). Review of active control of circular cylinder flow. *Ocean. Eng.* 258, 111840. doi:10.1016/j.oceaneng.2022.111840

Clapperton, B. L., and Bearman, P. W. (2018). Control of circular cylinder flow using distributed passive jets. *J. Fluid Mech.* 848, 1157–1178. doi:10.1017/jfm.2018.399

Constantinides, Y., and Oakley, Jr O. H. (2006). Numerical prediction of bare and straked cylinder VIV. *Int. Conf. offshore Mech. Arct. Eng. Hamburg* 4, 745–753. doi:10.1115/omae2006-92334

Das, S., Abishek, S., Balachandar, R., and Barron, R. M. (2023). Wake characteristics of wall-mounted solid and foam-covered circular cylinders. *Phys. Fluid* 35 (11). doi:10.1063/5.0169165

Derakhshandeh, J. F., and Alam, M. M. (2019). A review of bluff body wakes. *Ocean. Eng.* 182, 475–488. doi:10.1016/j.oceaneng.2019.04.093

Du, H., Zhang, Q., Li, Q., Kong, W., and Yang, L. (2022). Drag reduction in cylindrical wake flow using porous material. *Phys. Fluids* 34 (4), 045102. doi:10.1063/5.0085990

Duranay, A., Demirhan, A. E., Dobrucali, E., and Kinaci, O. K. (2023). A review on vortex-induced vibrations in confined flows. *Ocean. Eng.* 285, 115309. doi:10.1016/j.oceaneng.2023.115309

Edegbe, M., Nasif, G., and Balachandar, R. (2024). Wake characteristics of near-wall submerged bluff bodies with varying streamwise length. *Phy. Fluid* 36 (11). doi:10.1063/5.0239290

Eydi, F., Mojra, A., and Abdi, R. (2022). Comparative analysis of the flow control over a circular cylinder with detached flexible and rigid splitter plates. *Phy. Fluid* 34 (11). doi:10.1063/5.0110398

Firat, E., Ozkan, G. M., and Akilli, H. (2017). PIV measurements in the near wakes of hollow cylinders with holes. *Exp. Fluid* 58, 39–19. doi:10.1007/s00348-017-2334-x

Firat, E., Ozkan, G. M., and Akilli, H. (2019). Flow past a hollow cylinder with two spanwise rows of holes. *Exp. Fluid* 60, 163–217. doi:10.1007/s00348-019-2814-2

Forouzi Feshalami, B., He, S., Scarano, F., Gan, L., and Morton, C. (2022). A review of experiments on stationary bluff body wakes. *Phys. Fluids* 34 (1). doi:10.1063/5.0077323

Freitas, R. B., Brandão, P. V., Alves, L. S. B., Celli, M., and Barletta, A. (2022). The effect of local thermal non-equilibrium on the onset of thermal instability for a metallic foam. *Phys. Fluids* 34 (3), 034105. doi:10.1063/5.0083045

Fu, H., and Rockwell, D. (2005). Shallow flow past a cylinder: control of the near wake. *J. Fluid Mech.* 539, 1–24. doi:10.1017/s0022112004002666

Gao, D. L., Chen, W. L., Li, H., and Hu, H. (2017b). Flow around a slotted circular cylinder at various angles of attack. *Exp. Fluid* 58, 132–215. doi:10.1007/s00348-017-2417-8

Gao, D. L., Chen, W. L., Li, H., and Hu, H. (2017c). Flow around a circular cylinder with slit. *Exp. Therm. Fluid Sci.* 82, 287–301. doi:10.1016/j.expthermflusci.2016.11.025

Gao, Y., Fu, S., Ma, L., and Chen, Y. (2014). Experimental investigation of the response performance of VIV on a flexible riser with helical strakes. *Ships Offshore Struct.* 11, 113–128. doi:10.1080/17445302.2014.962788

Gao, Y., Yang, J., Xiong, Y., Wang, M., and Lu, D. (2017a). VIV response of a long flexible riser fitted with different helical strake coverages in uniform and linearly sheared currents. *Ships Offshore Struct* 12 (4), 575–590. doi:10.1080/17445302.2016.1187832

Hao, Z., Zhou, T., Wang, X., and Tan, S. K. (2010). Experimental studies of vortex structures in the wake of a cylinder with helical strakes. *Int. Conf. Offshore Mech. Arct. Eng.* 49149, 473–477. doi:10.1115/omae2010-20181

Heidari, M., Balachandar, R., Roussinova, V., and Barron, R. M. (2017). Characteristics of flow past a slender, emergent cylinder in shallow open channels. *Phys. Fluids* 29 (6), 065111. doi:10.1063/1.4986563

Hu, J., Hu, K., Zhang, Y., Yang, X., and Wu, S. (2023). Experiment and simulation investigation of flow characters in metal foam. *Numer. Heat. Transf. Part B* 83 (1–2), 24–38. doi:10.1080/10407790.2022.2105124

Huang, S. (2011). VIV suppression of a two-degree-of-freedom circular cylinder and drag reduction of a fixed circular cylinder by the use of helical grooves. *J. Fluids Struct.* 27 (7), 1124–1133. doi:10.1016/j.jfluidstructs.2011.07.005

Huang, S., and Sworn, A. (2013). Hydrodynamic coefficients of two fixed circular cylinders fitted with helical strakes at various staggered and tandem arrangements. *Appl. Ocean Res.* 43, 21–26. doi:10.1016/j.apor.2013.06.001

Huera-Huarte, F. (2024). Vortex-induced vibration of flexible cylinders in crossflow. *Annu. Rev. Fluid Mech.* 57, 285–310. doi:10.1146/annurev-fluid-022724-014235

Igarashi, T. (1978). Flow characteristics around a circular cylinder with a slit: 1st report, flow control and flow patterns. *Bull. JSME* 21 (154), 656–664. doi:10.1299/jsme1958.21.656

Igarashi, T. (1982). Flow characteristics around a circular cylinder with a slit: 2nd report, effect of boundary layer suction. *Bull. JSME* 25 (207), 1389–1397. doi:10.1299/jsme1958.25.1389

Ishihara, T., and Li, T. (2020). Numerical study on suppression of vortex-induced vibration of circular cylinder by helical wires. *J. Wind Eng. Ind. Aerodyn.* 197, 104081. doi:10.1016/j.jweia.2019.104081

Janocha, M. J., Ong, M. C., and Yin, G. (2022). Large eddy simulations and modal decomposition analysis of flow past a cylinder subject to flow-induced vibration. *Phy. Fluid* 34 (4). doi:10.1063/5.0084966

Jian Sheng, W., and Chen, W. (2016). Features of flow past a circular cylinder with a slit. *Sci. Iran.* 23 (5), 2097–2112. doi:10.24200/sci.2016.3941

Kawamura, T., Mayer, S., Garapon, A., and Sorensen, L. (2002). Large eddy simulation of a flow pasta free surface piercing circular cylinder. *J. Fluids Eng.* 124 (1), 91–101. doi:10.1115/1.1431545

Kim, J., Chae, S., and Kim, J. (2023). Flow control over a circular cylinder using a slot and axially arranged holes. *Ocean. Eng.* 287, 115794. doi:10.1016/j.oceaneng.2023.115794

Kingora, K., and Sadat, H. (2022). Flow and scalar transfer characteristics for a circular colony of vegetation. *Phy. Fluid* 34 (8). doi:10.1063/5.0090272

Klausmann, K., and Ruck, B. (2017). Drag reduction of circular cylinders by porous coating on the leeward side. *J. Fluid Mech.* 813, 382–411. doi:10.1017/jfm.2016.757

Korkischko, I., and Meneghini, J. R. (2010). Experimental investigation of flow-induced vibration on isolated and tandem circular cylinders fitted with strakes. *J. Fluids Struct.* 26 (4), 611–625. doi:10.1016/j.jfluidstructs.2010.03.001

Korkischko, I., and Meneghini, J. R. (2011). Volumetric reconstruction of the mean flow around circular cylinders fitted with strakes. *Exp. Fluids* 51 (4), 1109–1122. doi:10.1007/s00348-011-1127-x

Kusano, K. (2024). Aeroacoustic simulation of bluff bodies with protrusions at moderate Reynolds number. *Phy. Fluid* 36 (2). doi:10.1063/5.0186743

Lekkala, M. R., Latheef, M., Jung, J. H., Coraddu, A., Zhu, H., Srinil, N., et al. (2022). Recent advances in understanding the flow over bluff bodies with different geometries at moderate Reynolds numbers. *Ocean. Eng.* 261, 111611. doi:10.1016/j.oceaneng.2022.111611

Li, D., Liu, M., Huai, W., Liu, G., Peng, Z., and Zhang, F. (2023). Conditional statistics of Reynolds stress in open channel flows with modeled canopies of homogeneous and heterogeneous density. *Phy. Fluid* 35 (3). doi:10.1063/5.0141128

Li, Y., Gong, L., Ding, B., Xu, M., and Joshi, Y. (2021). Thermal management of power electronics with liquid cooled metal foam heat sink. *Int. J. Therm. Sci.* 163, 106796. doi:10.1016/j.ijthermalsci.2020.106796

Liu, H., Wei, J., and Qu, Z. (2014). The interaction of porous material coating with the near wake of bluff body. *J. Fluids Eng.* 136 (2), 021302. doi:10.1115/1.4026071

Liu, M., Huai, W., Ji, B., and Han, P. (2021). Numerical study on the drag characteristics of rigid submerged vegetation patches. *Phy. Fluid* 33 (8). doi:10.1063/5.0060601

Liu, M., Yang, Z., Ji, B., Huai, W., and Tang, H. (2022). Flow dynamics in lateral vegetation cavities constructed by an array of emergent vegetation patches along the open-channel bank. *Phy. Fluid* 34 (3). doi:10.1063/5.0084287

Ma, H. L., and Kuo, C. H. (2016). Control of boundary layer flow and lock-on of wake behind a circular cylinder with a normal slit. *Eur. J. Mech.-B/Fluids* 59, 99–114. doi:10.1016/j.euromechflu.2016.05.001

Ma, L., Lin, K., Fan, D., Wang, J., and Triantafyllou, M. S. (2022). Flexible cylinder flow-induced vibration. *Phy. Fluid* 34 (1). doi:10.1063/5.0078418

Mittal, C., and Sharma, A. (2021). Flow-induced vibration of a flexible splitter-plate in the wake of a stationary cylinder. *Phy. Fluid* 33 (11). doi:10.1063/5.0071523

Muñoz-Hervás, J. C., Lorite-Díez, M., Ruiz-Rus, J., and Jiménez-González, J. I. (2024). Experimental study on the flow-induced vibrations of a circular cylinder with a rear flexibly hinged splitter plate. *Phy. Fluid* 36 (2). doi:10.1063/5.0184410

Murali, D., and Petha Sethuraman, V. R. (2024). Flow control using hot splitter plates in the wake of a circular cylinder: a hybrid strategy. *Phy. Fluid* 36 (1). doi:10.1063/5.0180008

Nguyen, Q. D., Lu, W., Chan, L., Ooi, A., and Lei, C, C. (2023). A state-of-the-art review of flows past confined circular cylinders. *Phys. Fluids* 35 (7). doi:10.1063/5.0157470

Odabaee, M., Hooman, K., and Gurgenci, H. (2011). Metal foam heat exchangers for heat transfer augmentation from a cylinder in crossflow. *Transp. Porous Med.* 86 (3), 911–923. doi:10.1007/s11242-010-9664-y

Olsen, J. F., and Rajagopalan, S. (2000). Vortex shedding behind modified circular cylinders. *J. Wind Eng. Ind. Aerodyn.* 86 (1), 55–63. doi:10.1016/s0167-6105(00)00003-9

Ordia, L., Venugopal, A., Agrawal, A., and Prabhu, S. V. (2017). Vortex shedding characteristics of a cylinder with a parallel slit placed in a circular pipe. *J. Vis.* 20, 263–275. doi:10.1007/s12650-016-0398-y

Peng, B. H., Miau, J. J., Bao, F., Weng, L. D., Chao, C. C., and Hsu, C. C. (2012). Performance of vortex shedding from a circular cylinder with a slit normal to the stream. *Flow. Meas. Instrumen.* 25, 54–62. doi:10.1016/j.flowmeasinst.2011.07.003

Pizer, S. M., Amburn, E. P., Austin, J. D., Cromartie, R., Geselowitz, A., Greer, T., et al. (1987). Adaptive histogram equalization and its variations. *Comput. Graph. Image Process.* 39 (3), 355–368. doi:10.1016/s0734-189x(87)80186-x

Priyadarsan, A., and Afzal, M. S. (2023). Numerical investigation of flow past a circular cylinder modified with a single groove at low Reynolds number. *Phy. Fluid* 35 (2). doi:10.1063/5.0137530

Quen, L. K., Abu, A., Kato, N., Muhamad, P., Sahekhaini, A., and Abdullah, H. (2014). Investigation on the effectiveness of helical strakes in suppressing VIV of flexible riser. *Appl. Ocean Res.* 44, 82–91. doi:10.1016/j.apor.2013.11.006

Quen, L. K., Abu, A., Kato, N., Muhamad, P., Tan, L. K., and Kang, H. S. (2018). Performance of two and three-start helical strakes in suppressing the vortex-induced vibration of a low mass ratio flexible cylinder. *Ocean. Eng.* 166, 253–261. doi:10.1016/j.oceaneng.2018.08.008

Ranjith, E. R., Sunil, A. S., and Pauly, L. (2016). Analysis of flow over a circular cylinder fitted with helical strakes. *Procedia Technol.* 24, 452–460. doi:10.1016/j.protcy.2016.05.062

Rastan, M. R., and Alam, M. M. (2021). Transition of wake flows past two circular or square cylinders in tandem. *Phy. Fluid* 33 (8). doi:10.1063/5.0062978

Ren, H., Xu, Y., Cheng, J., Cao, P., Zhang, M., Fu, S., et al. (2019b). Vortex-induced vibration of flexible pipe fitted with helical strakes in oscillatory flow. *Ocean. Eng.* 189, 106274. doi:10.1016/j.oceaneng.2019.106274

Ren, H., Xu, Y., Zhang, M., Fu, S., Meng, Y., and Huang, C. (2019a). Distribution of drag coefficients along a flexible pipe with helical strakes in uniform flow. *Ocean. Eng.* 184, 216–226. doi:10.1016/j.oceaneng.2019.05.038

Ren, H., Zhang, M., Cheng, J., Cao, P., Xu, Y., Fu, S., et al. (2020). Magnification of hydrodynamic coefficients on a flexible pipe fitted with helical strakes in oscillatory flows. *Ocean. Eng.* 210, 107543. doi:10.1016/j.oceaneng.2020.107543

Roy, D. K. S. (2023). Simulation of flow over a fixed and oscillating circular cylinder with different surface roughness patterns using a multi-block-multi-mesh framework immersed boundary method. *Phy. Fluid* 35 (11). doi:10.1063/5.0172658

Sahu, T. R., Chopra, G., and Mittal, S. (2024). Vortex-induced vibration of a circular cylinder in the supercritical regime. *Phy. Fluid* 36 (10). doi:10.1063/5.0229933

Sahu, T. R., Furquan, M., and Mittal, S. (2023). Symmetry-breaking response of a flexible splitter plate attached to a circular cylinder in uniform flow. *Phy. Fluid* 35 (12). doi:10.1063/5.0177041

Senga, H., and Larsen, C. M. (2017). Forced motion experiments using cylinders with helical strakes. *J. Fluids Struct.* 68, 279–294. doi:10.1016/j.jfluidstructs.2016.11.004

Sharma, B., and Barman, R. N. (2023). Unsteady flow past slotted circular cylinders in laminar regime: effect of slit shapes and Reynolds number. *Phy. Fluid* 35 (1). doi:10.1063/5.0130736

Sharma, B., Verma, G., and Barman, R. N. (2022). Steady flow of power-law fluids past a slotted circular cylinder at low Reynolds number. *Phy. Fluid* 34 (9). doi:10.1063/5.0102861

Shi, X. D., and Feng, L. H. (2015). Control of flow around a circular cylinder by bleed near the separation points. *Exp. Fluid* 56, 214–217. doi:10.1007/s00348-015-2083-7

Sikdar, P., Dash, S. M., and Lua, K. B. (2024). Vortex structure manipulation and drag reduction of tandem circular cylinders using a pitching splitter plate. *Phy. Fluid* 36 (12). doi:10.1063/5.0242588

Sueki, T., Takaishi, T., Ikeda, M., and Arai, N. (2010). Application of porous material to reduce aerodynamic sound from bluff bodies. *Fluid Dyn. Res.* 42 (1), 015004. doi:10.1088/0169-5983/42/1/015004

Suh, J., Yang, J., and Stern, F. (2011). The effect of air–water interface on the vortex shedding from avertical circular cylinder. *J. Fluids Struct.* 27, 1–22. doi:10.1016/j.jfluidstructs.2010.09.001

Sui, J., Wang, J., Liang, S., and Tian, Q. (2016). VIV suppression for a large mass-damping cylinder attached with helical strakes. *J. Fluids Struct.* 62, 125–146. doi:10.1016/j.jfluidstructs.2016.01.005

Sumner, D. (2013). Flow above the free end of a surface-mounted finite-height circular cylinder: a review. *J. Fluids Struct.* 43, 41–63. doi:10.1016/j.jfluidstructs.2013.08.007

Sun, Y., Wang, J., Fan, D., Zheng, H., and Hu, Z. (2022). The roles of rigid splitter plates in flow-induced vibration of a circular cylinder. *Phy. Fluid* 34 (11). doi:10.1063/5.0126867

Taj, Z., Bista, S., Balachandar, R., and Barron, R. (2024). "Wake dynamics of flow past wall-mounted cylinder with cross-slot," in *Proceedings of the Canadian Society for mechanical engineering International Congress, 31st Annual Conference of the computational fluid dynamics Society of Canada* (Ontario, Canada).

Tanaka, N. (2022). Numerical investigation of 3D flow properties around finite emergent vegetation by using the two-phase volume of fluid (VOF) modeling technique. *Fluids* 7 (5), 175. doi:10.3390/fluids7050175

Tariq, H., Ghani, U., Anjum, N., and Pasha, G. A. (2022). 3D numerical modeling of flow characteristics in an open channel having in-line circular vegetation patches with varying density under submerged and emergent flow conditions. *J. Hydro. Hydromech.* 70 (1), 128–144. doi:10.2478/johh-2021-0034

Terekhov, V. I. (2021). Heat transfer in highly turbulent separated flows: a review. *Energies* 14 (4), 1005. doi:10.3390/en14041005

Thakurta, A., and Balachandar, R. (2025). On the wake dynamics of wall-mounted helical straked cylinders. *Phys. Fluids* 37 (1). doi:10.1063/5.0250201

Thielicke, W., and Stamhuis, E. (2014). PIVlab – towards user-friendly, affordable and accurate digital particle image velocimetry in MATLAB. *J. Open Res. Softw.* 2 (1), e30. doi:10.5334/jors.bl

Thompson, M. C., Leweke, T., and Hourigan, K. (2021). Bluff bodies and wake–wall interactions. *Annu. Rev. Fluid Mech.* 53 (1), 347–376. doi:10.1146/annurev-fluid-072220-123637

Wang, C., and Li, Y. (2023). Control of a circular cylinder flow using attached solid/perforated splitter plates at deflection angles. *Phy. Fluid* 35 (10). doi:10.1063/5.0165632

Wang, H. F., and Zhou, Y. (2009). The finite-length square cylinder near wake. *J. Fluid Mech.* 638, 453–490. doi:10.1017/s0022112009990693

Wang, H. F., Zhou, Y., Chan, C. K., and Lam, K. S. (2006). Effect of initial conditions on interaction between a boundary layer and a wall-mounted finite-length-cylinder wake. *Phys. Fluids* 18 (6), 065106. doi:10.1063/1.2212329

Wang, J., and Dong, Y. (2017). The numerical investigation of flow and heat transfer characteristics of flow past a slit-cylinder. *Sci. China Tech. Sci.* 60, 602–612. doi:10.1007/s11431-016-0375-8

Wang, J., and Wang, C. (2016). Heat transfer and flow characteristics of a rectangular channel with a small circular cylinder having slit-vent vortex generator. *Int. J. Therm. Sci.* 104, 158–171. doi:10.1016/j.ijthermalsci.2016.01.006

Westerweel, J., and Scarano, F. (2005). Universal outlier detection for PIV data. *Exp. Fluids* 39, 1096–1100. doi:10.1007/s00348-005-0016-6

Wu, Y., Cheng, Z., McConkey, R., Lien, F. S., and Yee, E. (2022). Modelling of flow-induced vibration of bluff bodies: a comprehensive survey and future prospects. *Energies* 15 (22), 8719. doi:10.3390/en15228719

Xia, C., Wei, Z., Yuan, H., Li, Q., and Yang, Z. (2018). POD analysis of the wake behind a circular cylinder coated with porous media. *J. Vis.* 21, 965–985. doi:10.1007/s12650-018-0511-5

Xiao, J., and Jing, D. (2024). Fluid flow and mixing in a channel with dual bluff bodies. *Phy. Fluid* 36 (1). doi:10.1063/5.0187211

Xu, C., Wang, C., Mao, Y., and Jiang, S. (2023). Experimental studies on pressure drag and aerodynamic noise of cylinder with porous coatings. *Phys. Fluids* 35 (6), 065123. doi:10.1063/5.0153779

Xu, W. H., and Ma, Y. X. (2024). A review on vibration control of multiple cylinders subjected to flow-induced vibrations. *China Ocean. Eng.* 38 (2), 183–197. doi:10.1007/s13344-024-0016-z

Xu, W. H., Yang, M., Ai, H. N., He, M., and Li, M. H. (2020). Application of helical strakes for suppressing the flow-induced vibration of two side-by-side long flexible cylinders. *China Ocean. Eng.* 34 (2), 172–184. doi:10.1007/s13344-020-0017-5

Yadegari, M., Khoshnevis, A. B., and Boloki, M. (2023). An experimental investigation of the effects of helical strakes on the characteristics of the wake around the circular cylinder. *Iran. J. Sci. Technol. Trans. Mech. Eng.* 47 (1), 67–80. doi:10.1007/s40997-022-00494-0

Yajima, Y., and Sano, O. (1996). A note on the drag reduction of a circular cylinder due to double rows of holes. *Fluid Dyn. Res.* 18 (4), 237–243. doi:10.1016/0169-5983(96)00015-9

Yu, H., Hu, H., Chen, W. L., Lu, Y., and Gao, D. (2024). Flow modulation mechanism in a cylinder with corrugated surfaces. *Phy. Fluid* 36 (1). doi:10.1063/5.0176679

Yuan, H., Xia, C., Chen, Y., and Yang, Z. (2016). "Flow around a finite circular cylinder coated with porous media," in *Proceedings of the 8th International Colloquium on bluff body aerodynamics and applications* (Boston, Massachusetts).

Zeng, L., Zhao, F., Wang, H., Liu, Y., and Tang, H. (2023). Control of flow-induced vibration of a circular cylinder using a splitter plate. *Phy. Fluid* 35 (8). doi:10.1063/5.0160114

Zhao, M. (2023). A review of recent studies on the control of vortex-induced vibration of circular cylinders. *Ocean. Eng.* 285, 115389. doi:10.1016/j.oceaneng.2023.115389

Zhao, M., Mamoon, A. A., and Wu, H. (2021). Numerical study of the flow past two wall-mounted finite-length square cylinders in tandem arrangement. *Phy. Fluid* 33 (9). doi:10.1063/5.0058394

Zheng, C., Zhou, P., Zhong, S., and Zhang, X. (2023). On the cylinder noise and drag reductions in different Reynolds number ranges using surface pattern fabrics. *Phy. Fluid* 35 (3). doi:10.1063/5.0138074

Zhou, T., Razali, S. M., and Cheng, L. (2010). Investigation on suppression of vortex-induced vibration using helical strakes. *Int. Conf. Offshore Mech. Arct. Eng.* 49149, 891–900. doi:10.1115/omae2010-20984

Zhou, T., Razali, S. M., Hao, Z., and Cheng, L. (2011). On the study of vortex-induced vibration of a cylinder with helical strakes. *J. Fluids Struct.* 27 (7), 903–917. doi:10.1016/j.jfluidstructs.2011.04.014

Zhu, H., Chen, Q., Tang, T., Alam, M. M., Zhou, T., and Zhong, J. (2023). Flow-induced response and wake characteristics of a flexible splitter plate attached to a circular cylinder in laminar flow. *Phy. Fluid* 35 (12). doi:10.1063/5.0180616

Zhu, H., Chen, Q., Zhong, J., and Zhou, W. Z. T. (2024). Wake-induced response of a flexible splitter plate detachedly placed downstream of a circular cylinder. *Phy. Fluid* 36 (7). doi:10.1063/5.0217046

Zhu, H., Zhao, H., and Zhou, T. (2019). Direct numerical simulation of flow over a slotted cylinder at low Reynolds number. *Appl. Ocean Res.* 87, 9–25. doi:10.1016/j.apor.2019.01.019

Zong, L., and Nepf, H. (2012). Vortex development behind a finite porous obstruction in a channel. *J. Fluid Mech.* 691, 368–391. doi:10.1017/jfm.2011.479